

## Second round review

We thank the Referee #2 again for his review. To facilitate the review process we have copied the reviewer comments in black text. Our responses are in regular blue font. We have responded to all the referee comments and made alterations to our paper (**in bold text**). Page and line numbers refer to the *first revised* manuscript.

### Referee #2

The authors have largely addressed my concerns in their rebuttal. I am happy that the paper can form the basis of ongoing discussions in the field of OFR deployment and interpretation. I am particularly satisfied with the RTD analysis and its explanation of the deviation from plug flow. I am still slightly concerned by the continued separation of the gaseous and condensed phase processes. I am in full agreement with the authors that "OFR modeling is a subfield in itself, and our group cannot be expected to address every single possible topic". However, where a process can have a substantial influence on the processes that are the subject of a manuscript, then this possibility should be acknowledged.

It can be argued that the two statements in point 2.2 of the authors response:

- i) "The presence of aerosols has typically negligible impacts on the gas-phase chemistry" and
- ii) "...gas-phase species have only limited impacts on OA"

are not demonstrably correct for all conditions in OFRs.

R2.5) To rebut i), consider the typical concentrations in diesel emissions. Concentrations of NO<sub>x</sub> in raw diesel exhaust are typically between 50 and 1000 ppm depending on running conditions and technology (and can be very much higher during transients and below 17 degrees C when EGR is not mandated). Clearly this is the sort of NO<sub>x</sub> target regime of the current manuscript. Whilst PM emissions do not respond in the same way as NO<sub>x</sub> to engine technologies (e.g. EGR generally increases PM whilst decreasing NO<sub>x</sub>, and only DPF fitted vehicles have significantly reduced PM) or load-speed conditions, typical concentrations from a modern light-duty (EURO5) diesel generally range from between 1 and 30 mg/m<sup>3</sup> in raw exhaust. Assuming 80 nm modal diameter, 1 mg/m<sup>3</sup> will provide a mass transfer rate ("condensation sink") of about 4 s<sup>-1</sup> (using an uptake coefficient of unity); so a lifetime of 0.25 s for such a condensing gas (and 30 mg/m<sup>3</sup> would give a lifetime of less than 0.01 s). A lower uptake coefficient would obviously lead to a longer lifetime (e.g. 1 s for 0.01 at 30 mg/m<sup>3</sup>).

Lines 88 to 92 explicitly include OFR conditions where there is a substantial likelihood of such high primary PM mass (an urban tunnel, "where NO<sub>x</sub> was high enough to be a major OH reactant"... and ... emissions of vehicles, biomass burning, and other combustion sources, "where NO can often be hundreds of ppm"). Looking at the Karjalainen et al., 2016 case presented in Figures 7 and 8, the authors are carrying out calculations under raw, 12 x and 100 x dilution

conditions for gasoline engine emissions. Figure 7 in Karjalainen reported average primary PM values of 0.45 mg/m<sup>3</sup> for parts of the test cycle (assumed raw), rising to more than 10 mg/m<sup>3</sup> including the SOA from a gasoline engine. Similarly, the Link et al., 2016 study of diesel emissions at 45 - 110 dilution employed no primary particle removal technology to emissions from a turbocharged, intercooled, heavy-duty, off-road diesel engine likely to emit massively more than the light-duty levels stated above (in excess of 100 mg/m<sup>3</sup> is readily possible in raw exhaust from such engines). In both these cases the mass transfer of potentially condensing closed shell and radical species to PM could clearly provide very significant sinks of gaseous components that should be considered in a model of OFRs.

We realize that the Referee is not understanding what we intended to communicate with our statements. When we stated that the “gas-phase chemistry” was not significantly perturbed by the presence of particles, we were referring to the gas-phase chemistry that we are modeling, i.e., the radical and NO<sub>x</sub>-NO<sub>y</sub> chemistry, as well as the consumption of VOCs and other OH reactants. We did not intend to include the physical partitioning of semivolatile and low volatility species, which clearly is an area of strong interaction of the gas and particle phases (but for the most part does not involve chemistry). We will clarify the language, as described below, to remove this potential source of confusion.

We thank the Referee for providing detailed examples for high condensational sink in combustion exhausts. Nevertheless, even if raw exhausts are injected into the reactor, they still cannot have significant impacts on the major gas-phase oxidants, since VOCs and NO<sub>x</sub> in raw exhausts, which are also proportionally higher, still dominate total oxidant sink. Dilution of raw exhausts simultaneously lowers condensational sinks and gas-phase reactive oxidant sinks, with their relative importance remaining the same.

We have added a few sentences to clarify this point at the end of the paragraph i) in L151. The modified paragraph now reads:

- i) **“The presence of aerosols has typically negligible impacts on the gas-phase chemistry of radicals, NO<sub>x</sub>/NO<sub>y</sub>, and OH reactants studied here. Condensational sink (CS) of ambient aerosols can rarely exceed 1 s<sup>-1</sup> even in polluted areas and is usually 1-3 orders of magnitude lower (Donahue et al., 2016; Palm et al., 2016). Thus, even under the assumption of unity uptake coefficient, CS cannot compete with OHR<sub>ext</sub> (usually on the order of 10 s<sup>-1</sup> or higher) in OH loss. Uptake of NO onto aerosols only occurs through the reaction with RO<sub>2</sub> on particle surface (Richards-Henderson et al., 2015), which is formed very slowly (see below) compared to gas-phase HO<sub>x</sub> and NO<sub>x</sub> chemistry. Uptake of HO<sub>2</sub>, O<sub>3</sub>, NO<sub>3</sub> etc. is even more unlikely to be of importance due to lower uptake coefficients (Moise and Rudich, 2002; Moise et al., 2002; Hearn and Smith, 2004; Lakey et al., 2015). Combustion exhausts can have high aerosol loadings with condensational sinks on the order of 10<sup>2</sup>–10<sup>3</sup> s<sup>-1</sup> (Matti Maricq, 2007). Even if these exhausts are directly injected into the reactor without any pre-treatment, uptake onto the particles still cannot play a major role in the fate of gas-phase radical and NO<sub>x</sub> species, since VOCs and NO<sub>x</sub> in raw exhausts, which are**

**proportionally orders-of-magnitude higher, still dominate the fate of oxidants. Dilution of combustion emissions simultaneously lowers condensational sinks and the sinks of oxidants due to chemical reactions, with their relative importance remaining the same as in undiluted emissions.”**

We acknowledge that a strong dilution leads to a lower PM loading than in raw exhausts, which slows down the uptake. But this “lower” PM loading may still be much higher than typical ambient values after dilution. So it may not necessarily be “low PM loading” compared to ambient conditions, as suggested by the Referee below (R2.8).

We have added some text to L566 to acknowledge the PM loading change by dilution:

**“Note that a strong dilution lowers aerosol mass loading in vehicle emissions. As a result, condensation of gases onto particles is slower than in raw exhausts. However, condensational sinks after dilution may still be significantly higher than typical ambient values (Matti Maricq, 2007; Donahue et al., 2016).”**

R2.6) To address author response 2.2 ii), clearly gas-phase species have a strong impact on OA, being 100% responsible for all SOA. Mass transfer of semi-volatile and low volatility gas-phase species (in the case of exhaust experiments, almost completely due to condensation on existing primary PM) has a determinant effect on PM mass. Gas phase oxidants may have a limited impact on OA chemistry, but gas phase species have a profound effect on OA. Given the paper title relates to modelling the chemistry in OFRs (not modelling the oxidants), it is not solely transfer of radical species between phases that is of concern.

As discussed in response to R2.5, we agree with this and did not intend to say otherwise. However this mostly concerns physics (“mass transfer” in the Referee’s words) and not chemistry. We have modified that paragraph to clarify the fact that physical uptake of semivolatile and low-volatility gas-phase species have a strong impact on PM mass:

- ii) **“Gas-phase radical and  $\text{NO}_x/\text{NO}_y$  species only has limited impacts on OA chemistry in this study. Heterogeneous oxidation of OA by OH is generally slow. Significant OA loss due to heterogeneous oxidation can only be seen at equivalent photochemical ages as high as weeks (Hu et al., 2016). The enhancement of heterogeneous oxidation due to NO is remarkable only at OH concentration close to the ambient values but not at typical values in OFR (Richards-Henderson et al., 2015).**

**It is well known that the aerosol concentration can have a major impact on the physical uptake of semivolatile and low-volatility gas-phase species. However this process is not explicitly modeled in this study.”**

Also, we have modified text to L148 for more clarity:

**“Also, particle-phase chemistry and physical and chemical interactions of gas-phase species with particles are not considered in this study.”**

R2.7) In the context of the above discussion, I do not understand the final paragraph of the authors suggested added text in point 2.2. I think this requires further explanation before inclusion in the paper.

The core idea of that paragraph is that the details of VOC product evolution have a strong influence on the rate of OH loss, but this is highly complex and not well captured even by models as explicit as MCM. We surrogated VOC evolution by SO<sub>2</sub> for simplicity and efficiency and this introduces much more uncertainty on (the temporal variation of) OHR<sub>ext</sub> due to VOC (and hence the radical chemistry) than mass transfer to the particle phase does. Thus, there is no strong need for explicitly including gas-particle mass transfer in the present modeling work.

We have modified that paragraph (L166) below for more clarity:

**“As OHR<sub>ext</sub> plays a major and even dominant role in OH loss, it is an important approximation that the *real* OHR<sub>ext</sub> decay (due to not only primary VOC oxidation and subsequent oxidation of higher generation products, but also wall loss, partitioning to the particle phase, reactive uptake etc.) is surrogated by that of SO<sub>2</sub> (see Fig. S2 of Peng et al. 2015). Gas-phase measurements in literature laboratory studies revealed that there is a large variability of the evolution of total OHR<sub>ext</sub> during oxidation of primary VOCs and subsequent oxidation of their intermediate products, depending on the type of precursors (Nehr et al., 2014; Schwantes et al., 2017). This variability is obviously mainly due to the formation of different types and amounts of oxidation intermediates/products contributing to OHR<sub>ext</sub>. This variation is highly complex due to the large number of possible oxidation intermediates and the limited knowledge of detailed higher-generation mechanisms, and thus is difficult to accurately capture even if modeling with a mechanism as explicit as Master Chemical Mechanism is performed (Schwantes et al., 2017). Therefore, it is justified to use a lumped surrogate to model the OHR<sub>ext</sub> decay for simplicity and efficiency. This approximation is a major contributor to uncertainty of our model. The uncertainties due to both the types of oxidation intermediates/products.”**

R2.8) Whilst I do not expect the paper to explicitly address coupling of the gaseous and particulate processes, I would expect the current manuscript to at least acknowledge the interaction between the gas phase chemistry and gaseous losses associated with condensation and the resultant increase in PM mass. The authors should state that their study is completely relevant for low PM loadings in OFRs, but care should be taken when applying it to high ambient PM concentration or direct emission studies (both raw and diluted). Clearly the authors are aware of the necessity to include coupled multiphase processes and should be commended in their work with Jeff Pierce's group on this.

We have acknowledged (see the response to R2.5) that dilution changes PM loadings and hence mass transfer rates, and, when diluted, sources have lower PM loadings in OFRs than in raw emissions. However, we believe that the statement that our study is only valid to low PM loadings is incorrect, as discussed in detail in our response to R2.5. Thus no changes have been made in response to this point.

## References

Donahue, N. M., Posner, L. N., Westervelt, D. M., Li, Z., Shrivastava, M., Presto, A. A., Sullivan, R. C., Adams, P. J., Pandis, S. N. and Robinson, A. L.: Where Did This Particle Come From? Sources of Particle Number and Mass for Human Exposure Estimates, in *Airborne Particulate Matter: Sources, Atmospheric Processes and Health*, edited by R. M. Harrison, R. E. Hester, and X. Querol, pp. 35–71, Royal Society of Chemistry., 2016.

Hearn, J. D. and Smith, G. D.: Kinetics and Product Studies for Ozonolysis Reactions of Organic Particles Using Aerosol CIMS †, *J. Phys. Chem. A*, 108(45), 10019–10029, doi:10.1021/jp0404145, 2004.

Hu, W., Palm, B. B., Day, D. A., Campuzano-Jost, P., Krechmer, J. E., Peng, Z., de Sá, S. S., Martin, S. T., Alexander, M. L., Baumann, K., Hacker, L., Kiendler-Scharr, A., Koss, A. R., de Gouw, J. A., Goldstein, A. H., Seco, R., Sjostedt, S. J., Park, J.-H., Guenther, A. B., Kim, S., Canonaco, F., Prévôt, A. S. H., Brune, W. H. and Jimenez, J. L.: Volatility and lifetime against OH heterogeneous reaction of ambient isoprene-epoxydiols-derived secondary organic aerosol (IEPOX-SOA), *Atmos. Chem. Phys.*, 16(18), 11563–11580, doi:10.5194/acp-16-11563-2016, 2016.

Lakey, P. S. J., George, I. J., Whalley, L. K., Baeza-Romero, M. T. and Heard, D. E.: Measurements of the HO<sub>2</sub> Uptake Coefficients onto Single Component Organic Aerosols, *Environ. Sci. Technol.*, 49(8), 4878–4885, doi:10.1021/acs.est.5b00948, 2015.

Matti Maricq, M.: Chemical characterization of particulate emissions from diesel engines: A review, *J. Aerosol Sci.*, 38(11), 1079–1118, doi:10.1016/j.jaerosci.2007.08.001, 2007.

Moise, T. and Rudich, Y.: Reactive Uptake of Ozone by Aerosol-Associated Unsaturated Fatty Acids: Kinetics, Mechanism, and Products, *J. Phys. Chem. A*, 106(27), 6469–6476, doi:10.1021/jp025597e, 2002.

Moise, T., Talukdar, R. K., Frost, G. J., Fox, R. W. and Rudich, Y.: Reactive uptake of NO<sub>3</sub> by liquid and frozen organics, *J. Geophys. Res.*, 107(D2), 4014, doi:10.1029/2001JD000334, 2002.

Nehr, S., Bohn, B., Fuchs, H., Häsel, R., Hofzumahaus, A., Li, X., Rohrer, F., Tillmann, R. and Wahner, A.: Atmospheric photochemistry of aromatic hydrocarbons: OH budgets during SAPHIR chamber experiments, *Atmos. Chem. Phys.*, 14(13), 6941–6952, doi:10.5194/acp-14-6941-2014, 2014.

Palm, B. B., Campuzano-Jost, P., Ortega, A. M., Day, D. A., Kaser, L., Jud, W., Karl, T., Hansel, A., Hunter, J. F., Cross, E. S., Kroll, J. H., Peng, Z., Brune, W. H. and Jimenez, J. L.: In situ secondary organic aerosol formation from ambient pine forest air using an oxidation flow reactor, *Atmos. Chem. Phys.*, 16(5), 2943–2970, doi:10.5194/acp-16-2943-2016, 2016.

Peng, Z., Day, D. A., Stark, H., Li, R., Lee-Taylor, J., Palm, B. B., Brune, W. H. and Jimenez, J. L.: HO<sub>x</sub> radical chemistry in oxidation flow reactors with low-pressure mercury lamps systematically examined by modeling, *Atmos. Meas. Tech.*, 8(11), 4863–4890, doi:10.5194/amt-8-4863-2015, 2015.

Richards-Henderson, N. K., Goldstein, A. H. and Wilson, K. R.: Large Enhancement in the Heterogeneous Oxidation Rate of Organic Aerosols by Hydroxyl Radicals in the Presence of Nitric Oxide, *J. Phys. Chem. Lett.*, 6, 4451–4455, doi:10.1021/acs.jpcclett.5b02121, 2015.

Schwantes, R. H., Schilling, K. A., McVay, R. C., Lignell, H., Coggon, M. M., Zhang, X., Wennberg, P. O. and Seinfeld, J. H.: Formation of highly oxygenated low-volatility products from cresol oxidation, *Atmos. Chem. Phys.*, 17(5), 3453–3474, doi:10.5194/acp-17-3453-2017, 2017.

1 **Modeling of the chemistry in oxidation flow reactors with high initial NO**

2 Zhe Peng and Jose L. Jimenez

3 Cooperative Institute for Research in Environmental Sciences and Department of Chemistry, University of  
4 Colorado, Boulder, CO 80309, USA

5 Correspondence to: J.L. Jimenez (jose.jimenez@colorado.edu)

6

7 **Abstract.** Oxidation flow reactors (OFRs) are increasingly employed in atmospheric chemistry research  
8 because of their high efficiency of OH radical production from low-pressure Hg lamp emissions at both  
9 185 and 254 nm (OFR185) or 254 nm only (OFR254). OFRs have been thought to be limited to studying  
10 low-NO chemistry (where peroxy radicals ( $RO_2$ ) react preferentially with  $HO_2$ ) because NO is very rapidly  
11 oxidized by the high concentrations of  $O_3$ ,  $HO_2$ , and OH in OFRs. However, many groups are performing  
12 experiments aging combustion exhaust with high NO levels, or adding NO in the hopes of simulating  
13 high-NO chemistry (where  $RO_2 + NO$  dominates). This work systematically explores the chemistry in  
14 OFRs with high initial NO. Using box modeling, we investigate the interconversion of N-containing  
15 species and the uncertainties due to kinetic parameters. Simple initial injection of NO in OFR185 can  
16 result in more  $RO_2$  reacted with NO than with  $HO_2$  and minor non-tropospheric photolysis, but only  
17 under a very narrow set of conditions (high water mixing ratio, low UV intensity, low external OH  
18 reactivity ( $OHR_{ext}$ ), and initial NO concentration ( $NO^{in}$ ) of tens to hundreds of ppb) that account for a  
19 very small fraction of the input parameter space. These conditions are generally far away from  
20 experimental conditions of published OFR studies with high initial NO. In particular, studies of aerosol  
21 formation from vehicle emissions in OFR often used  $OHR_{ext}$  and  $NO^{in}$  several orders of magnitude higher.  
22 Due to extremely high  $OHR_{ext}$  and  $NO^{in}$ , some studies may have resulted in substantial non-tropospheric  
23 photolysis, strong delay to  $RO_2$  chemistry due to peroxyxynitrate formation, VOC reactions with  $NO_3$   
24 dominating over those with OH, and faster reactions of OH-aromatic adducts with  $NO_2$  than those with  
25  $O_2$ , all of which are irrelevant to ambient VOC photooxidation chemistry. Some of the negative effects  
26 are worst for alkene and aromatic precursors. To avoid undesired chemistry, vehicle emissions generally  
27 need to be diluted by a factor of  $>100$  before being injected into OFR. However, sufficiently diluted  
28 vehicle emissions generally do not lead to high-NO chemistry in OFR, but are rather dominated by the  
29 low-NO  $RO_2+HO_2$  pathway. To ensure high-NO conditions without substantial atmospherically irrelevant  
30 chemistry in a more controlled fashion, new techniques are needed.

31 **1 Introduction**

32 The oxidation of gases that are emitted into the atmosphere, in particular volatile organic  
33 compounds (VOCs), is one of the most important atmospheric chemistry processes (Haagen-Smit, 1952;  
34 Chameides et al., 1988). VOC oxidation is closely related to radical production and consumption (Levy  
35 II, 1971), O<sub>3</sub> production, and formation of secondary aerosols (Odum et al., 1996; Hoffmann et al., 1997;  
36 Volkamer et al., 2006; Hallquist et al., 2009), which have impacts on air quality and climate (Lippmann,  
37 1991; Nel, 2005; Stocker et al., 2014).

38 Chemical reactors are critical tools for research of VOC oxidation. Oxidation reactions of interest  
39 often have typical timescales of hours to weeks. Studying these processes in ambient air can be  
40 confounded by dispersion and changes in ambient conditions, which often occur on similar timescales.  
41 Chemical reactors allow for decoupling of these two types of processes. Also, they should be able to  
42 simulate the different regimes of reactions occurring in the atmosphere, e.g., VOC oxidation under low  
43 and high-NO conditions (peroxy radical fate dominated by reaction with HO<sub>2</sub> or with NO) representing  
44 remote and urban areas, respectively (Orlando and Tyndall, 2012).

45 Large environmental chambers are a commonly used reactor type (Carter et al., 2005; Wang et al.,  
46 2011). They typically employ actinic wavelength (>300 nm) light sources (e.g., outdoor solar radiation  
47 and UV blacklights) to produce oxidants and radicals and have large volumes (on the order of several  
48 cubic meters or larger). However, the capability of generating sustained elevated levels of OH, the most  
49 important tropospheric oxidant, is usually limited in chambers, resulting in OH concentrations similar  
50 to those in the atmosphere (10<sup>6</sup>–10<sup>7</sup> molecules cm<sup>-3</sup>; Mao et al., 2009; Ng et al., 2010), and consequently,  
51 long simulation times (typically hours) to reach OH equivalent ages of atmospheric relevance (George  
52 et al., 2007; Kang et al., 2007; Carlton et al., 2009; Seakins, 2010; Wang et al., 2011). The partitioning of  
53 gases and aerosols to chamber walls (usually made of Teflon) in timescales of tens of minutes to hours  
54 makes it difficult to conduct very long experiments that simulate high atmospherically-relevant  
55 photochemical ages (Cocker et al., 2001; Matsunaga and Ziemann, 2010; Zhang et al., 2014; Krechmer  
56 et al., 2016). In addition, the long simulation times and large size of chambers and auxiliary equipment  
57 are logistically difficult for field deployment, and their cost limits the number of laboratories equipped  
58 with them.

59 Given the limitations of environmental chambers, a growing number of experimenters have  
60 instead employed oxidation flow reactors (OFRs). OFRs have a much smaller size (of the order of 10 L),  
61 efficiently generate OH via photolysis of H<sub>2</sub>O and/or O<sub>3</sub> by more energetic 185 and 254 nm photons  
62 from low-pressure Hg lamps, and overcome the abovementioned shortcomings of chambers due to a  
63 much shorter residence time (George et al., 2007; Kang et al., 2007, 2011; Lambe et al., 2011). Moreover,  
64 OFRs are able to rapidly explore a wide range of OH equivalent ages within a short period (~2 hr), during  
65 which significant changes of ambient conditions can usually be avoided in the case of field deployment  
66 (Ortega et al., 2016; Palm et al., 2016, 2017). Because of these advantages, OFRs have recently been  
67 widely used to study atmospheric chemistry, in particular secondary organic aerosol (SOA) formation  
68 and aging, in both the laboratory and the field (Kang et al., 2011; Li et al., 2013; Ortega et al., 2013,



69 2016; Tkacik et al., 2014; Palm et al., 2016).

70 In addition to experimental studies using OFRs, there has also been some progress in the  
71 characterization of OFR chemistry by modeling. Li et al. (2015) and Peng et al. (2015) developed a box  
72 model for OFR HO<sub>x</sub> chemistry that predicts measurable quantities [e.g., OH exposure (OH<sub>exp</sub>, in  
73 molecules cm<sup>-3</sup> s) and O<sub>3</sub> concentration (abbr. O<sub>3</sub> hereinafter, in ppm)] in good agreement with  
74 experiments. This model has been used to characterize HO<sub>x</sub> chemistry as a function of H<sub>2</sub>O mixing ratio  
75 (abbr. H<sub>2</sub>O hereinafter, unitless), UV light intensity (abbr. UV hereinafter, in photons cm<sup>-2</sup> s<sup>-1</sup>), and  
76 external OH reactivity [in s<sup>-1</sup>, OHR<sub>ext</sub>=∑k<sub>i</sub>C<sub>i</sub>, i.e., the sum of the products of concentrations of externally  
77 introduced OH-consuming species (C<sub>i</sub>) and rate constants of their reactions with OH (k<sub>i</sub>)]. Based on this  
78 characterization, Peng et al. (2015) found that OH suppression, i.e., reduction of OH concentration  
79 caused by OHR<sub>ext</sub>, is a common feature under many typical OFR operation conditions. Peng et al. (2016)  
80 systematically examined the relative importance of non-OH/non-tropospheric reactants on the fate of  
81 VOCs over a wide range of conditions, and provided guidelines for OFR operation to avoid non-  
82 tropospheric VOC photolysis, i.e., VOC photolysis at 185 and 254 nm.

83 In previous OFR modeling studies, NO<sub>x</sub> chemistry was not investigated in detail, since in such in  
84 typical OFR experiments with large amounts of oxidants (e.g., OH, HO<sub>2</sub>, and O<sub>3</sub>), NO would be very  
85 rapidly oxidized and thus unable to compete with HO<sub>2</sub> for reaction with peroxy radicals (RO<sub>2</sub>). Li et al.  
86 (2015) estimated an NO (NO<sub>2</sub>) lifetime of ~0.5 (~1.5) s under a typical OFR condition. From these  
87 estimates, OFRs processing ambient air or laboratory air without large addition of NO<sub>x</sub> were assumed  
88 to be not suitable for studying oxidation mechanisms relevant to polluted conditions under higher NO  
89 concentrations. OFRs have recently been used to conduct laboratory experiments with very high initial  
90 NO<sub>x</sub> levels (Liu et al., 2015) and deployed to an urban tunnel, where NO<sub>x</sub> was high enough to be a major  
91 OH reactant (Tkacik et al., 2014). The former study reported evidence for the incorporation of nitrogen  
92 into SOA. Besides, OFRs have been increasingly employed to process emissions of vehicles, biomass  
93 burning, and other combustion sources (Table 1), where NO can often be hundreds of ppm (Ortega et  
94 al., 2013; Martinsson et al., 2015; Karjalainen et al., 2016; Link et al., 2016; Schill et al., 2016; Alanen et  
95 al., 2017; Simonen et al., 2017). It can be expected that such a high NO input together with very high  
96 VOC concentrations would cause a substantial deviation from good OFR operation conditions identified  
97 in Peng et al. (2016). Very recently, N<sub>2</sub>O injection has been proposed by Lambe et al. (2017) as a way to  
98 study oxidation of VOCs under high NO conditions in OFR. As more OFR studies at high NO<sub>x</sub> level are  
99 conducted, there is growing need to understand the chemistry of N-containing species in OFRs and  
100 whether it proceeds along atmospherically-relevant channels.

101 In this study, we present the first comprehensive model of OFR NO<sub>y</sub> chemistry. We extend the  
102 model of Li et al. (2015) and Peng et al. (2015) by including a scheme for NO<sub>y</sub> species. Then this model  
103 is used to investigate i) if an OFR with initial NO injection results in NO significantly reacting with RO<sub>2</sub>  
104 under any conditions, ii) if previously published OFR experiments with high initial NO concentrations  
105 led to RO<sub>2</sub>+NO being dominant in VOC oxidation without negative side effects (e.g., non-tropospheric  
106 reactions), iii) how to avoid undesired chemistry in future studies. The results can provide insights into

107 the design and interpretation of future OH-oxidation OFR experiments with large amounts of NO<sub>x</sub>  
108 injection.

## 109 **2 Methods**

110 The physical design of the OFR modeled in the present work, the chemical kinetics box model, and  
111 the method of propagating and analyzing the parametric uncertainties on the model have already been  
112 introduced previously (Kang et al., 2007; Li et al., 2015; Peng et al., 2015). We only provide brief  
113 descriptions for them below.

### 114 **2.1 Potential Aerosol Mass flow reactor**

115 The OFR modeled in this study is the “Potential Aerosol Mass” (PAM) flow reactor, firstly  
116 introduced by Kang et al. (2007). The PAM OFR is a cylindrical vessel with a volume of ~13 L, equipped  
117 with low-pressure Hg lamps (model no. 82-9304-03, BHK Inc.) to generate 185 and 254 nm UV light.  
118 This popular design is being used by many atmospheric chemistry research groups, particularly those  
119 studying SOA (Lambe and Jimenez, 2017 and references therein). When the lamps are mounted inside  
120 Teflon sleeves, photons at both wavelengths are transmitted and contribute to OH production (“OFR185  
121 mode”). In OFR185, H<sub>2</sub>O photolyzed at 185 nm produces OH and HO<sub>2</sub>, while O<sub>2</sub> photolyzed at the same  
122 wavelengths results in O<sub>3</sub> formation. O(<sup>1</sup>D) is produced via O<sub>3</sub> photolysis at 254 nm and generates  
123 additional OH through its reaction with H<sub>2</sub>O. 185 nm lamp emissions can be filtered by mounting the  
124 lamps inside quartz sleeves, leaving only 254 nm photons to produce OH (“OFR254 mode”). In this mode,  
125 injection of externally formed O<sub>3</sub> is necessary to ensure OH production. As the amount of O<sub>3</sub> injected is  
126 a key parameter under some conditions (Peng et al., 2015), we adopt the notation OFR254-X to denote  
127 OFR254 experiments with X ppm initial O<sub>3</sub> (O<sub>3,in</sub>). In this study, we investigate OFR experiments with NO  
128 injected and thus utilize “OFR185-iNO” to describe the OFR185 mode of operation with initially (at the  
129 reactor entrance) injected NO. The same terminology is used for the OFR254 mode. For instance, the  
130 initial NO injection into OFR254-7 is denoted as OFR254-7-iNO.

### 131 **2.2 Model description**

132 The basic framework of the box model used in this study, a standard chemical kinetics model, is  
133 the same as in Peng et al. (2015). Plug flow is assumed in the model, since approximately taking  
134 residence time distribution into account leads to similar results under most conditions but at much  
135 higher computational expense (Peng et al., 2015). In addition to the reactions in the model of Peng et  
136 al. (2015), including all HO<sub>x</sub> reactions available in the JPL Chemical Kinetic Data Evaluation (Sander et al.,  
137 2011), all gas-phase NO<sub>y</sub> reactions available in the JPL database except those of organic nitrates and  
138 peroxy nitrates are also considered in the current reaction scheme. An updated JPL evaluation was  
139 published recently (Burkholder et al., 2015), with slightly different (~20%) rate constants for  
140 NO<sub>2</sub>+HO<sub>2</sub>+M→HO<sub>2</sub>NO<sub>2</sub>+M and NO<sub>2</sub>+NO<sub>3</sub>→N<sub>2</sub>O<sub>5</sub>. The updated rate constants only result in changes of  
141 ~10–20% of the concentrations of the species directly consumed/produced by these reactions. These  
142 changes are smaller than the parametric uncertainties of the model (see Section 3.1.3). For other  
143 species, concentration changes are negligible. HO<sub>2</sub>NO<sub>2</sub>+M→HO<sub>2</sub>+NO<sub>2</sub>+M and N<sub>2</sub>O<sub>5</sub>+M→NO<sub>2</sub>+NO<sub>3</sub>+M,  
144 are also included in the scheme, with kinetic parameters from the IUPAC Task Group on Atmospheric

145 Chemical Kinetic Data Evaluation (Ammann et al., 2016). As in Peng et al. (2015, 2016), SO<sub>2</sub> is used as a  
146 surrogate of external OH reactants (e.g., VOCs). NO<sub>y</sub> species, although also external OH reactants, are  
147 explicitly treated in the model and *not* counted in OHR<sub>ext</sub> in this work. Therefore, OHR<sub>ext</sub> stands for *non*-  
148 NO<sub>y</sub> OHR<sub>ext</sub> only hereinafter, unless otherwise stated.

149 Also, particle-phase chemistry and physical and chemical interactions of gas-phase species with  
150 particles are not considered in this study. We have made this assumption because:

151 i) The presence of aerosols has typically negligible impacts on the gas-phase chemistry of radicals,  
152 NO<sub>y</sub>/NO<sub>x</sub>, and OH reactants studied here. Condensational sink (CS) of ambient aerosols can  
153 rarely exceed 1 s<sup>-1</sup> even in polluted areas and is usually 1-3 orders of magnitude lower  
154 (Donahue et al., 2016; Palm et al., 2016). Thus, even under the assumption of unity uptake  
155 coefficient, CS cannot compete with OHR<sub>ext</sub> (usually on the order of 10 s<sup>-1</sup> or higher) in OH loss.  
156 Uptake of NO onto aerosols only occurs through the reaction with RO<sub>2</sub> on particle surface  
157 (Richards-Henderson et al., 2015), which is formed very slowly (see below) compared to gas-  
158 phase HO<sub>x</sub> and NO<sub>x</sub> chemistry. Uptake of HO<sub>2</sub>, O<sub>3</sub>, NO<sub>3</sub> etc. is even more unlikely to be of  
159 importance due to lower uptake coefficients (Moise and Rudich, 2002; Moise et al., 2002;  
160 Hearn and Smith, 2004; Lakey et al., 2015). Combustion exhausts can have high aerosol  
161 loadings with condensational sinks on the order of 10<sup>2</sup>–10<sup>3</sup> s<sup>-1</sup> (Matti Maricq, 2007). Even if  
162 these exhausts are directly injected into the reactor without any pre-treatment, uptake onto  
163 the particles still cannot play a major role in the fate of gas-phase radical and NO<sub>x</sub> species, since  
164 VOCs and NO<sub>x</sub> in raw exhausts, which are proportionally orders-of-magnitude higher, still  
165 dominate the fate of oxidants. Dilution of combustion emissions simultaneously lowers  
166 condensational sinks and the sinks of oxidants due to chemical reactions, with their relative  
167 importance remaining the same as in undiluted emissions.

168 ii) Gas-phase radical and NO<sub>y</sub>/NO<sub>x</sub> species only has limited impacts on OA chemistry in this study.  
169 Heterogeneous oxidation of OA by OH is generally slow. Significant OA loss due to  
170 heterogeneous oxidation can only be seen at photochemical ages as high as weeks (Hu et al.,  
171 2016). The enhancement of heterogeneous oxidation due to NO is remarkable only at OH  
172 concentration close to the ambient values but not at typical values in OFR (Richards-Henderson  
173 et al., 2015).

174 It is well known that the aerosol concentration can have a major impact on the physical uptake of  
175 semivolatile and low-volatility gas-phase species. However this process is not explicitly modeled in this  
176 study.

177 As OHR<sub>ext</sub> plays a major and even dominant role in OH loss, it is an important approximation that  
178 the *real* OHR<sub>ext</sub> decay (due to not only primary VOC oxidation and subsequent oxidation of higher  
179 generation products, but also wall loss, partitioning to the particle phase, reactive uptake etc.) is  
180 surrogated by that of SO<sub>2</sub> (see Fig. S2 of Peng et al. 2015). Gas-phase measurements in literature  
181 laboratory studies revealed that there is a large variability of the evolution of total OHR<sub>ext</sub> during  
182 oxidation of primary VOCs and subsequent oxidation of their intermediate products, depending on the

Deleted: Also, particle-phase processes and interactions of gas-phase species with particles are not considered in this study. We have made this assumption because:

Deleted: efficient

Deleted: On the other hand, gas

Deleted: have

Deleted: It

Deleted: .

Deleted: (subsequent)

192 type of precursors (Nehr et al., 2014; Schwantes et al., 2017). This variability is obviously mainly due to  
193 the formation of different types and amounts of oxidation intermediates/products contributing to  
194  $\text{OHR}_{\text{ext}}$ . This variation is highly complex due to the large number of possible oxidation intermediates and  
195 the limited knowledge of detailed higher-generation mechanisms, and thus is difficult to accurately  
196 capture even if modeling with a mechanism as explicit as Master Chemical Mechanism is performed  
197 (Schwantes et al., 2017). Therefore, it is justified to use a lumped surrogate to model the  $\text{OHR}_{\text{ext}}$  decay  
198 for simplicity and efficiency. This approximation is a major contributor to uncertainty of our model. The  
199 uncertainties due to both the types of oxidation intermediates/products,

200 A residence time of 180 s and typical temperature (295 K) and atmospheric pressure (835 mbar)  
201 in Boulder, CO, USA are assumed for all model cases. The lower-than-sea level pressure only leads to  
202 minor differences in the outputs (Li et al., 2015). We explore physical input cases evenly spaced in a  
203 logarithmic scale over very wide ranges:  $\text{H}_2\text{O}$  of 0.07%–2.3%, i.e., relative humidity (RH) of 2–71% at  
204 295 K; 185 nm UV of  $1.0 \times 10^{11}$ – $1.0 \times 10^{14}$  and 254 nm UV of  $4.2 \times 10^{13}$ – $8.5 \times 10^{15}$  photons  $\text{cm}^{-2} \text{s}^{-1}$ ;  $\text{OHR}_{\text{ext}}$  of  
205 1–16000  $\text{s}^{-1}$ ;  $\text{O}_{3,\text{in}}$  of 2.2–70 ppm for OFR254; initial NO mixing ratio ( $\text{NO}^{\text{in}}$ ) from 10 ppt to 40 ppm.  
206 Besides, conditions with  $\text{OHR}_{\text{ext}}=0$  are also explored. UV at 254 nm is estimated from that at 185 nm  
207 according to the relationship determined by Li et al. (2015). Several typical cases within this range as  
208 well as their corresponding 4 or 2-character labels (e.g., MM0V and HL) are defined in Table 2. Literature  
209 studies are modeled by adopting all reported parameters (e.g., residence time,  $\text{H}_2\text{O}$ , and  $\text{O}_{3,\text{in}}$ ) and  
210 estimating any others that may be needed (e.g., UV) from the information provided in the papers.

211 In this study, OH equivalent ages are calculated under the assumption of an ambient OH  
212 concentration of  $1.5 \times 10^6$  molecules  $\text{cm}^{-3}$  (Mao et al., 2009). Conditions leading to a ratio of  $\text{RO}_2$  reacted  
213 with NO over the entire residence time [ $r(\text{RO}_2+\text{NO})$ ] to that with  $\text{HO}_2$  [ $r(\text{RO}_2+\text{HO}_2)$ ] larger than 1 are  
214 regarded as “high NO” (under the assumption of constant  $\text{OHR}_{\text{ext}}$  from VOCs, see Section S1 for more  
215 details), where [ $r(X)$ ] is the total reactive flux for reaction X over the entire residence time.  $F_{185_{\text{exp}}}/\text{OH}_{\text{exp}}$   
216 and  $F_{254_{\text{exp}}}/\text{OH}_{\text{exp}}$  are used as measures of the relative importance of VOC photolysis at 185 and 254  
217 nm to their reactions with OH, respectively [ $F_{185_{\text{exp}}}$  ( $F_{254_{\text{exp}}}$ ) are 185 (254) nm photon flux exposure,  
218 i.e., product of 185 (254) nm photon flux and time]. Readers may refer to Figs. 1 and 2 of Peng et al.  
219 (2016) for the determination of the relative importance of non-tropospheric (185 and 254 nm)  
220 photolysis of individual VOCs. Although the relative importance of non-tropospheric photolysis depends  
221 on individual VOCs, in the present work, we set criteria on  $F_{185_{\text{exp}}}/\text{OH}_{\text{exp}} < 3 \times 10^3$  cm/s and  
222  $F_{254_{\text{exp}}}/\text{OH}_{\text{exp}} < 4 \times 10^5$  cm/s to define “good” conditions and  $F_{185_{\text{exp}}}/\text{OH}_{\text{exp}} < 1 \times 10^5$  cm/s and  
223  $F_{254_{\text{exp}}}/\text{OH}_{\text{exp}} < 1 \times 10^7$  cm/s (excluding good conditions) to define “risky” conditions. Conditions with  
224 higher  $F_{185_{\text{exp}}}/\text{OH}_{\text{exp}}$  or  $F_{254_{\text{exp}}}/\text{OH}_{\text{exp}}$  are defined as “bad”. Under good conditions, photolysis of most  
225 VOCs has a relative contribution  $< 20\%$  to their fate; under bad conditions, non-tropospheric photolysis  
226 is likely to be significant in all OFR experiments, since it can hardly be avoided for oxidation  
227 intermediates, even if the precursor(s) does not photolyze at all. Under risky conditions, some species  
228 photolyzing slowly and/or reacting with OH rapidly (e.g., alkanes, aldehydes, and most biogenics) still  
229 have a relative contribution of photolysis  $< 20\%$  to their fates, while species photolyzing more rapidly

Deleted: evolution

Deleted: , but not

Deleted: changes in CS, wall conditions etc. Also this variability

Deleted: MCM

Deleted: It

Deleted: thus

Deleted: introduced by this approximation include those

Deleted: and all interactions of VOCs with aerosols, walls etc. And the uncertainties due to the former dominate over those due to the latter

240 and/or reacting with OH more slowly (e.g., aromatics and other highly conjugated species and some  
241 saturated carbonyls) will undergo substantial non-tropospheric photolysis. Note that these definitions  
242 are slightly different than in Peng et al. (2016). All definitions of the types of conditions are summarized  
243 in Table 3.

### 244 **2.3 Uncertainty analysis**

245 We apply the same method as in Peng et al. (2014, 2015) to calculate and analyze the output  
246 uncertainties due to uncertain kinetic parameters in the model. Random samples following log-normal  
247 distributions are generated for all rate constants and photoabsorption cross sections in the model using  
248 uncertainty data available in the JPL database (Sander et al., 2011) or estimated based on IUPAC data  
249 (Ammann et al., 2016). Then, Monte Carlo Uncertainty Propagation (BIPM et al., 2008) is performed for  
250 these samples through the model to obtain the distributions of outputs. Finally, we compute squared  
251 correlation coefficients between corresponding input and output samples and apportion the relative  
252 contributions of individual kinetic parameters to the output uncertainties based on these coefficients  
253 (Saltelli et al., 2005).

## 254 **3 Results and discussion**

255 In this section, we study the NO<sub>y</sub> chemistry in OFR while considering relevant experimental issues.  
256 Based on these results, we propose some guidelines for OFR operation for high-NO OH oxidation of  
257 VOCs.

### 258 **3.1 NO<sub>y</sub> chemistry in typical OFR cases with initial NO injection**

259 NO was thought to be unimportant (i.e., unable to significantly react with RO<sub>2</sub>) in OFRs with initial  
260 NO injection (OFR-iNO) based on the argument that its lifetime is too short due to large amounts of O<sub>3</sub>  
261 OH, and HO<sub>2</sub> to compete with RO<sub>2</sub>+HO<sub>2</sub> (Li et al., 2015). We evaluate this issue below by calculating NO  
262 effective lifetime ( $\tau_{NO}$ , in s), defined as NO exposure (NO<sub>exp</sub>, in molecules cm<sup>-3</sup> s) divided by initial NO  
263 concentration, under various conditions. This definition cannot effectively capture the true NO average  
264 lifetime if it is close to or longer than the residence time. In this case,  $\tau_{NO}$  close to the residence time  
265 will be obtained, which is still long enough for our characterization purposes.

#### 266 **3.1.1 OFR185-iNO**

267 In OFR185-iNO, NO is *not* oxidized extremely quickly under *all* conditions. For instance, under a  
268 typical condition in the midrange of the phase space shown in Fig. 1a,  $\tau_{NO} \sim 13$  s. This lifetime is much  
269 shorter than the residence time, but long enough for OH<sub>exp</sub> to reach  $\sim 3 \times 10^{10}$  molecules cm<sup>-3</sup> s, which is  
270 equivalent to an OH equivalent age of  $\sim 6$  hrs. Such an OH equivalent age is already sufficient to allow  
271 some VOC processing and even SOA formation to occur (Lambe et al., 2011; Ortega et al., 2016). Within  
272  $\tau_{NO}$ , NO suppresses HO<sub>2</sub> through the reaction NO+HO<sub>2</sub>→NO<sub>2</sub>+OH, leading to NO<sub>exp</sub>/HO<sub>2exp</sub> of  $\sim 700$  during  
273 this period, high enough for RO<sub>2</sub> to dominantly react with NO. Meanwhile, NO+HO<sub>2</sub>→NO<sub>2</sub>+OH enhances  
274 OH production, which helps OH<sub>exp</sub> build up in a relatively short period. In addition, non-tropospheric  
275 photolysis of VOCs at 185 and 254 nm is minor (F185<sub>exp</sub>/OH<sub>exp</sub>  $\sim 600$  cm/s, Fig. 1a), because of enhanced  
276 OH production and moderate UV. Therefore, such an OFR condition may be of some interest for high-  
277 NO VOC oxidation. We thus analyze the NO<sub>y</sub> chemistry in OFR185-iNO in more detail below, by taking

278 the case shown in Fig. 1a as a representative example.

279 In OFR185-iNO, HO<sub>x</sub> concentrations are orders-of-magnitude higher than in the atmosphere  
280 while the amount of O<sub>3</sub> produced is relatively small during the first several seconds after the flow enters  
281 the reactor. As a result, NO is not oxidized almost exclusively by O<sub>3</sub> as in the troposphere, but also by  
282 OH and HO<sub>2</sub> to form HONO and NO<sub>2</sub>, respectively (Fig. 1a). The large concentration of OH present then  
283 oxidizes HONO to NO<sub>2</sub>, and NO<sub>2</sub> to HNO<sub>3</sub>. Photolysis only plays a negligible role in the fate of HONO and  
284 NO<sub>2</sub> in OFRs, in contrast to the troposphere, where it is the main fate of these species. This is because  
285 the reactions of HONO and NO<sub>2</sub> with OH are greatly accelerated in OFR compared to those in the  
286 troposphere, while photolysis not (Peng et al., 2016). The interconversion between NO<sub>2</sub> and HO<sub>2</sub>NO<sub>2</sub> is  
287 also greatly accelerated (Fig. 1a), since a large amount of HO<sub>2</sub> promotes the formation of HO<sub>2</sub>NO<sub>2</sub>,  
288 whose thermal decomposition and reaction with OH in turn enhance the recycling of NO<sub>2</sub>. Though not  
289 explicitly modeled in this study, RO<sub>2</sub> are expected to undergo similar reactions with NO<sub>2</sub> to form  
290 reservoir species, i.e., peroxy nitrates (Orlando and Tyndall, 2012). Peroxy nitrates that decompose on  
291 timescales considerably longer than OFR residence times may serve as effectively permanent NO<sub>y</sub> sinks  
292 in OFRs (see Section 3.4.1).

293 Interestingly but not surprisingly, the NO<sub>y</sub> chemistry shown in Fig. 1a is far from temporally  
294 uniform during the OFR residence time (Fig. S1a). Within  $\tau_{NO}$ , NO undergoes an e-fold decay as it is  
295 rapidly converted into NO<sub>2</sub> and HONO, whose concentrations reach maxima around that time. After  
296 most NO is consumed, HONO and NO<sub>2</sub> also start to decrease, but significantly more slowly than NO,  
297 since they do not have as many and efficient loss pathways as NO. The reaction of OH with HONO, the  
298 dominant fate of HONO, is slower than that with NO (Fig. 1a). The net rate of the NO<sub>2</sub>-to-HO<sub>2</sub>NO<sub>2</sub>  
299 conversion becomes low because of the relatively fast reverse reaction (Fig. 1a). Besides, the total loss  
300 of NO<sub>2</sub> is partially offset by the production from HONO. The generally stable concentrations of HONO  
301 and NO<sub>2</sub> (Fig. S1a) result in their respective reaction rates with OH that are comparable during and after  
302  $\tau_{NO}$  (Fig. 1a), as OH variation is also relatively small during the entire residence time (Fig. S1b). However,  
303 the NO<sub>2</sub>-to-HO<sub>2</sub>NO<sub>2</sub> conversion after  $\tau_{NO}$  is much faster than during it (Fig. 1a), resulting from  
304 substantially decreased NO and HO<sub>2</sub> concomitantly increasing >1 order of magnitude after  $\tau_{NO}$  (Fig.  
305 S1a,b). HNO<sub>3</sub> and HO<sub>2</sub>NO<sub>2</sub>, which are substantially produced only after NO<sub>2</sub> is built up, have much higher  
306 concentrations later than within  $\tau_{NO}$ .

307 Under other OFR185-iNO conditions than in Fig. 1a, the major reactions interconverting NO<sub>y</sub>  
308 species are generally the same, although their relative importance may vary. At lower NO<sup>in</sup>, the  
309 perturbation of HO<sub>x</sub> chemistry caused by NO<sub>y</sub> species is smaller. Effects of NO<sup>in</sup> less than 1 ppb (e.g.,  
310 typical non-urban ambient concentrations) are generally negligible regarding HO<sub>x</sub> chemistry. Regarding  
311 NO<sub>y</sub> species, the pathways in Fig. 1a are still important under those conditions. At higher NO<sup>in</sup> (e.g., >1  
312 ppm), one might expect NO<sub>3</sub> and N<sub>2</sub>O<sub>5</sub> to play a role (as in OFR254-iNO; see Section 3.1.2 below), since  
313 high NO<sub>y</sub> concentrations might enhance self/cross reactions of NO<sub>y</sub>. However, this would not occur  
314 unless OH production is high, since relatively low O<sub>3</sub> concentrations in OFR185-iNO cannot oxidize NO<sub>2</sub>  
315 to NO<sub>3</sub> rapidly. Also, a large amount of NO<sub>y</sub> can lead to significant OH suppression. That would in turn

316 slow down the  $\text{NO}_3$  production from  $\text{HNO}_3$  by OH. This is especially true when an OFR is used to oxidize  
317 the output of highly concentrated sources (e.g., from vehicle exhausts). When sources corresponding  
318 to  $\text{OHR}_{\text{ext}}$  of thousands of  $\text{s}^{-1}$  and  $\text{NO}^{\text{in}}$  of tens of ppm are injected into OFR185 (Fig. 1b), they essentially  
319 inhibit active chemistry except NO consumption, as all subsequent products are much less abundant  
320 compared to remaining NO (Fig. S1c).

### 321 3.1.2 OFR254-iNO

322 The ppm-level  $\text{O}_{3,\text{in}}$  used in the OFR254-iNO mode of operation has a strong impact on its  $\text{NO}_y$   
323 chemistry. An  $\text{O}_{3,\text{in}}$  of 2.2 ppm (lowest in this study) is already enough to shorten  $\tau_{\text{NO}}$  to  $\sim 1$  s, preventing  
324 NO from playing a role in the chemistry under most explored conditions. The reaction fluxes under a  
325 typical  $\text{O}_{3,\text{in}}$  of 7 ppm are shown in Fig. 1c. A reactive flux from  $\text{NO} + \text{O}_3 \rightarrow \text{NO}_2$  makes the reaction of NO  
326 with other oxidants (OH,  $\text{HO}_2$  etc.) negligible. The  $\text{HNO}_3$  production pathway from  $\text{NO}_2$  is similar to that  
327 in OFR185-iNO. The interconversion between  $\text{NO}_2$  and  $\text{HO}_2\text{NO}_2$  is also fast over the residence time, and  
328 even faster than in OFR185-iNO during  $\tau_{\text{NO}}$ , since a high concentration of  $\text{O}_3$  also controls the OH- $\text{HO}_2$   
329 interconversion and makes  $\text{HO}_2$  more resilient against suppression due to high NO (Fig. S1f; Peng et al.,  
330 2015). A major difference in the  $\text{NO}_y$  chemistry in OFR254-iNO (Fig. 1c) compared to OFR185-iNO (Fig.  
331 1a) is significant  $\text{NO}_3/\text{N}_2\text{O}_5$  chemistry due to high  $\text{O}_3$  in OFR254-iNO, which accelerates the oxidation of  
332  $\text{NO}_2$  to  $\text{NO}_3$ . Interconversion between  $\text{NO}_2 + \text{NO}_3$  and  $\text{N}_2\text{O}_5$  also occurs to a significant extent because of  
333 high  $\text{NO}_2$ . Under the conditions of Fig. 1c,  $\text{NO}_3$  can also be significantly consumed by  $\text{HO}_2$ . Unlike  
334 OFR185-iNO, OFR254-iNO can substantially form  $\text{NO}_3$  from  $\text{HNO}_3$  under conditions that are not on the  
335 extremes of the explored physical condition space, e.g., at higher UV and lower  $\text{NO}^{\text{in}}$  (e.g., Fig. S2). In  
336 the case of very high  $\text{NO}^{\text{in}}$  (equal to or higher than  $\text{O}_{3,\text{in}}$ ), all  $\text{O}_3$  can be rapidly destroyed by NO. As a  
337 consequence, OH production is shut down and these cases are of little practical interest (Fig. S3h).

### 338 3.1.3 Uncertainty analysis

339 The results of uncertainty propagation confirm that the output uncertainties due to uncertain  
340 kinetic parameters are relatively low compared to other factors (e.g., non-plug flow in OFR; Peng et al.,  
341 2015) and the overall model accuracy compared to experimental data (a factor of 2–3; Li et al., 2015).  
342 For OFR185-iNO, NO,  $\text{NO}_3$ , and OH exposures have relative uncertainties of  $\sim 0$ –20%,  $\sim 40$ –70%, and  $\sim 15$ –  
343 40%, respectively. The uncertainties in OH exposure are very similar to those in the cases without  $\text{NO}_x$   
344 (Peng et al., 2015). The contribution of NO<sub>y</sub> reactions to  $\text{OH}_{\text{exp}}$  uncertainty is negligible, except for some  
345 contribution of  $\text{OH} + \text{NO} \rightarrow \text{HONO}$  in a few cases with high  $\text{NO}^{\text{in}}$  (Fig. 2). The uncertainties on  $\text{NO}_{\text{exp}}$  are  
346 dominated by the reactions producing  $\text{HO}_x$  and  $\text{O}_3$ , i.e., the major consumers of NO. For  $\text{NO}_3$  exposure,  
347 a few major production and loss pathways (e.g.,  $\text{NO}_2 + \text{NO}_3 \rightarrow \text{N}_2\text{O}_5$ ,  $\text{N}_2\text{O}_5 \rightarrow \text{NO}_2 + \text{NO}_3$ , and  
348  $\text{HO}_2 + \text{NO}_3 \rightarrow \text{OH} + \text{NO}_2 + \text{O}_2$ ) dominate its uncertainties. OFR254-iNO has a simpler picture of parametric  
349 uncertainties in terms of composition.  $\text{O}_3$  controls the NO oxidation under most conditions and this  
350 reaction contributes most of output uncertainties for NO exposures.  $\text{HO}_2 + \text{NO}_3 \rightarrow \text{OH} + \text{NO}_2 + \text{O}_2$  dominates  
351 the uncertainty on  $\text{NO}_3$  exposure. The levels of those uncertainties are lower than in OFR185-iNO (<2%  
352 for NO exposure; <60% in all cases and <25% in most cases for  $\text{NO}_3$  exposure). Thus, model uncertainties  
353 in OFR254-iNO are not shown in detail.

### 354 3.2 Different conditions types

355 Having illustrated the main NO<sub>y</sub> chemical pathways for typical cases, we present the results of  
356 the exploration of the entire physical parameter space (see Section 2.2). Note that the explored space  
357 is indeed very large and gridded logarithmically uniformly in every dimension. Therefore, the statistics  
358 of the exploration results can be useful to determine the relative importance of the conditions types  
359 defined in Section 2.2 and Table 3.

360 It has been shown that during  $\tau_{NO}$ , RO<sub>2</sub> can react dominantly with NO (Section 3.1.1), while to  
361 determine if a condition is high-NO (see Table 3), the entire residence time is considered. This is done  
362 because for VOC oxidation systems of interest, there will be significant oxidation of the initial VOC and  
363 its products under low-NO conditions, if  $\tau_{NO}$  is shorter than the reactor residence time. After most NO  
364 is consumed, the longer the remaining residence time, the more RO<sub>2</sub> will react with HO<sub>2</sub> and the more  
365 likely that an input condition is classified as low-NO. For a condition to be high-NO, a significantly long  
366  $\tau_{NO}$  is required. Figure 3 shows the fractional occurrence distribution of good/risky/bad conditions in  
367 the entire explored condition space over logarithm of  $r(\text{RO}_2+\text{NO})/r(\text{RO}_2+\text{HO}_2)$ , which distinguishes high-  
368 and low-NO conditions. In OFR254-iNO,  $\tau_{NO}$  is so short that no good high-NO condition is found in the  
369 explored range in this study (Fig. 3a). A fraction of explored conditions are bad high-NO. These  
370 conditions result from a full consumption of O<sub>3</sub> by NO. Then very little HO<sub>x</sub> is produced (right panels in  
371 Fig. S3h), but the fate of any RO<sub>2</sub> formed is dominated by RO<sub>2</sub>+NO (right panels in Fig. S3i). However,  
372 also due to negligibly low OH concentration, little RO<sub>2</sub> is produced and non-tropospheric photolysis of  
373 VOCs is also substantial compared to their reaction with OH under these conditions, classifying all of  
374 them as “bad” (Fig. 3a).

375 In OFR185-iNO, in addition to the typical case shown in Fig. 1a, many other cases have a  $\tau_{NO}$  of  
376  $\sim 10$  s or longer (Figs. S3b and S4), which allow the possibility of high-NO conditions. Indeed,  $\sim 1/3$  of  
377 explored conditions in OFR185-iNO with a residence time of 3 min are high-NO (Fig. 3b). Most of these  
378 high-NO conditions are also classified as bad, similar with those in OFR254-iNO. More importantly, in  
379 contrast to OFR254-iNO, good and risky high-NO conditions also comprise an appreciable fraction of  
380 the OFR185-iNO conditions. It is easily expected that very high OHR<sub>ext</sub> and NO<sup>in</sup> lead to bad high-NO  
381 conditions (all panels in Fig. 4), since they strongly suppress HO<sub>x</sub>, which yields bad conditions and in  
382 turn keep NO destruction relatively low. Besides, the occurrence of bad high-NO conditions is reduced  
383 at high UV (bottom panels in Fig. 4), which can be explained by lowered NO due to high O<sub>3</sub> production  
384 and fast OH reactant loss due to high OH production. Good high-NO conditions are rare in the explored  
385 space. They are only 1.1% of total explored conditions (Fig. 3b) and present under very specific  
386 conditions, i.e., higher H<sub>2</sub>O, lower UV, lower OHR<sub>ext</sub>, and NO<sup>in</sup> of tens to hundreds of ppb (Figs. 4 and  
387 S5). Since a very high NO can suppress OH, to obtain both a significant NO level and a good conditions,  
388 NO<sup>in</sup> can only be tens to hundreds of ppb. As NO<sup>in</sup> is lower and OH is higher than under bad high-NO  
389 conditions, UV should be lower than bad high-NO conditions to keep a sufficiently long presence of NO.  
390 Thus, UV at 185 nm for good high-NO conditions are generally lower than  $10^{12}$  photons cm<sup>-2</sup> s<sup>-1</sup> (Fig. S5).  
391 In addition, a low OHR<sub>ext</sub> (generally  $< 50$  s<sup>-1</sup>) and a higher H<sub>2</sub>O (the higher the better, although there is



392 no apparent threshold) are also required for good high-NO conditions (Fig. S5), as Peng et al. (2016)  
393 pointed out. Risky high-NO conditions often occur between good and bad high-NO conditions, e.g., at  
394 lower  $\text{NO}^{\text{in}}$  than bad conditions (e.g., Cases ML, MM, HL, and HM in Fig. 4, see Table 2 for the typical  
395 case label code), at higher  $\text{OHR}_{\text{ext}}$  and/or  $\text{NO}^{\text{in}}$  than good conditions (e.g., Cases ML and MM), and at  
396 lower  $\text{H}_2\text{O}$  than good conditions (e.g., Case LL).

397 The trend of the distributions of good, risky, and bad low-NO conditions is generally in line with  
398 the analysis in Peng et al. (2016). For low-NO conditions,  $\text{NO}_y$  species can be simply regarded as external  
399 OH reactants, as in Peng et al. (2016). As  $\text{H}_2\text{O}$  decreases and/or  $\text{OHR}_{\text{ext}}$  or  $\text{NO}^{\text{in}}$  increases, a low-NO  
400 condition becomes worse (good→risky→bad) (Figs. 4 and 5). In OFR185-iNO, increasing UV generally  
401 makes a low-NO condition better because of an OH production enhancement (Fig. 4); while in OFR254-  
402 iNO, increasing UV generally makes a low-NO condition worse (Fig. 5), since at a higher UV, more  $\text{O}_3$  is  
403 destroyed and the resilience of OH to suppression is reduced.

404 As discussed above, the fraction of high-NO conditions also depends on OFR residence time. A  
405 shorter residence time is expected to generally lead to a larger fraction of high-NO conditions, since the  
406 time spent in the reaction for  $t > \tau_{\text{NO}}$  is significantly smaller. Thus, we also investigate an OFR185-iNO  
407 case with a residence time of 30 s. In Fig. 3b, compared to the case with a residence time of 3 min, the  
408 distributions of all condition types (good/risky/bad) of the 30 s residence time case shift toward higher  
409  $r(\text{RO}_2+\text{NO})/r(\text{RO}_2+\text{HO}_2)$ . Nevertheless, shortening the residence time also removes the period when the  
410 condition is better (i.e., less non-tropospheric photolysis), when external OH reactants have been  
411 partially consumed and OH suppression due to  $\text{OHR}_{\text{ext}}$  has been reduced later in the residence time. As  
412 a result, the fractions of good and risky conditions decrease (Fig. 3b). With the two effects (higher  
413  $r(\text{RO}_2+\text{NO})/r(\text{RO}_2+\text{HO}_2)$  and more significant non-tropospheric photolysis) combined, the fraction of  
414 good high-NO conditions increases by a factor of  $\sim 3$ . An even shorter residence time does not result in  
415 a larger good high-NO fraction, since the effect of enhancing non-tropospheric photolysis is even more  
416 apparent.

### 417 3.3 Effect of non-plug flow

418 We performed model runs where the only change with respect to our box model introduced in  
419 Section 2.2 is that the plug-flow assumption is replaced by the residence time distribution (RTD)  
420 measured by Lambe et al. (2011) (also see Fig. S8 of Peng et al. (2015)). The chemistry of different air  
421 parcels with different residence times is simulated by our box model and outputs are averaged over the  
422 RTD. Lateral diffusion between different air parcels is neglected in these simulations.

423  $\text{OH}_{\text{exp}}$  calculated from the mode with RTD ( $\text{OH}_{\text{exp,RTD}}$ ) is higher than that calculated from the plug-  
424 flow model ( $\text{OH}_{\text{exp,PF}}$ ) in both OFR185-iNO and OFR254-iNO (Table 4 and Fig. S6). Under most explored  
425 conditions deviations are relatively small, which leads to an overall positive deviation of  $\text{OH}_{\text{exp,RTD}}$  from  
426  $\text{OH}_{\text{exp,PF}}$  by  $\sim 2$  (within the uncertainties of the model and its application to real experimental systems).  
427 For OFR185-iNO, most conditions ( $\sim 90\%$ ) in the explored space lead to  $< 3$  differences between  $\text{OH}_{\text{exp,PF}}$   
428 and  $\text{OH}_{\text{exp,RTD}}$ , while for a small fraction of cases the differences can be larger (Fig. S6). The larger  
429 deviations are mainly present at high UV,  $\text{OHR}_{\text{ext}}$ , and  $\text{NO}^{\text{in}}$ , where conditions are generally “bad” and in

430 which experiments are of little atmospheric relevance. Under these specific conditions, external OH  
431 reactants and NO<sub>y</sub> can be substantially destroyed for the air parcels with residence times longer than  
432 the average, while this is not the case for the average residence time. This feature was already described  
433 by Peng et al. (2015) (see Fig. S10 of that study). Although only non-NO<sub>y</sub> external OH reactants were  
434 considered in that study, the results are the same. In the present study, a higher upper limit of the  
435 explored OHR<sub>ext</sub> range (compared to Peng et al., 2015, due to trying to simulate extremely high OHR<sub>ext</sub>  
436 used in some recent literature studies) large amounts of NO<sub>y</sub> and cause somewhat larger deviations. In  
437 OFR254-iNO, OH is less suppressed at high OHR<sub>ext</sub> and NO<sup>in</sup> than in OFR185-iNO because of high O<sub>3</sub>  
438 (Peng et al., 2015), OH<sub>exp,RTD</sub> deviations from OH<sub>exp,PF</sub> are also smaller (Table 4).

439 Based on the outputs of the model with RTD, similar mapping of the physical input space as Figs.  
440 4 and 5 can be done (Figs. S7 and S8). Overall, the mapping of the RTD model results is very similar with  
441 that of the plug-flow model. The conditions appear to be only slightly better in a few places of the  
442 explored space than those from the plug-flow model, which can be easily explained by the discussions  
443 above. Besides, the mapping in Figs. S7 and S8 also appear to be slightly more low-NO, for the same  
444 reasons discussed above. After NO is destroyed at long residence times, HO<sub>2</sub>, suppressed by NO, also  
445 recovers as OH.  $r(\text{RO}_2+\text{NO})/r(\text{RO}_2+\text{HO}_2)$  is obviously expected to be smaller than in the plug-flow model  
446 in general.

447 Note that most conditions that appear to be better in the RTD model results are already  
448 identified as bad by the plug-flow model. Those conditions look slightly better only because of their  
449 better *RTD-averaged*  $F185_{\text{exp}}/\text{OH}_{\text{exp}}$  and  $F254_{\text{exp}}/\text{OH}_{\text{exp}}$ . However, each of those cases is actually  
450 composed of both a better part at longer residence times and also a worse part at shorter residence  
451 times. Under those conditions, the reactor simultaneously works in two distinct regimes, one of which  
452 is bad due to heavy OH suppression. Such conditions are obviously not desirable for OFR operation.

### 453 3.4 Possible issues related to high-NO<sub>x</sub> levels

454 In the discussion above, we focused on obtaining high-NO conditions and considered only one  
455 experimental issue (non-tropospheric photolysis) that had been previously investigated in Peng et al.  
456 (2016) and is not specific for experiments with high NO injection. We discuss additional potential  
457 reasons why the OFR-iNO chemistry can deviate strongly from tropospheric conditions, as specifically  
458 related to high-NO<sub>x</sub> level in this subsection.

#### 459 3.4.1 NO<sub>2</sub>

460 NO<sub>2</sub> reacts with RO<sub>2</sub> to form peroxy nitrates, generally regarded as reservoir species in the  
461 atmosphere as most of them thermally decompose very quickly compared to atmospheric time scales.  
462 However, in OFRs, with residence times on the order of minutes, some peroxy nitrates may no longer be  
463 considered as fast decomposing. This is especially true for acylperoxy nitrates, whose lifetimes can be  
464 hours at room temperature (Orlando and Tyndall, 2012). Acylperoxy nitrates are essentially sinks instead  
465 of reservoirs in OFRs for both NO<sub>2</sub> and RO<sub>2</sub>. RO<sub>2</sub> is estimated to be as high as several ppb in OFRs by our  
466 model (e.g., ~6 ppb RO<sub>2</sub> in OFR185 at H<sub>2</sub>O=1%, UV at 185 nm=1x10<sup>13</sup> photons cm<sup>-2</sup> s<sup>-1</sup>, OHR<sub>ext</sub>=1000 s<sup>-1</sup>,  
467 and NO<sup>in</sup>=0), while high-NO experiments can yield far higher NO<sub>2</sub>. If all RO<sub>2</sub> were acylperoxy, the RO<sub>2</sub>

468 chemistry could be rapidly shut down by NO<sub>2</sub>, as rate constants of these RO<sub>2</sub> + NO<sub>2</sub> reactions are around  
469 10<sup>-11</sup> cm<sup>3</sup> molecule<sup>-1</sup> s<sup>-1</sup> (Orlando and Tyndall, 2012). Nevertheless, acylperoxy nitrates are not expected  
470 to typically be the dominant component of peroxy nitrates, since acyl radicals are not a direct oxidation  
471 product of most common VOCs and can only be formed after several steps of oxidation (Atkinson and  
472 Arey, 2003; Ziemann and Atkinson, 2012). Most alkylperoxy nitrates retain their short-lived reservoir  
473 characteristics in OFRs due to their relatively short thermal decomposition time scales (on the order of  
474 0.1 s; Orlando and Tyndall, 2012). Even so, OFR experiments can be seriously hampered at extremely  
475 high NO<sub>2</sub>. If NO<sub>2</sub> reaches ppm levels, the equilibrium between RO<sub>2</sub>+NO<sub>2</sub> and alkylperoxy nitrate  
476 (RO<sub>2</sub>+NO<sub>2</sub>↔RO<sub>2</sub>NO<sub>2</sub>) is greatly shifted toward the alkylperoxy nitrate side, as the forward and reverse  
477 rate constants are on the order of 10<sup>-12</sup> cm<sup>3</sup> molecule<sup>-1</sup> s<sup>-1</sup> and 1 s<sup>-1</sup>, respectively (Orlando and Tyndall,  
478 2012). This results in a substantial decrease in effective RO<sub>2</sub> concentration, or in other words, a  
479 substantial slow-down of RO<sub>2</sub> chemistry.

480 Parts per million levels of NO<sub>2</sub> may impose an additional experimental artifact in the oxidation  
481 chemistry of aromatic precursors. OH-aromatic adducts, i.e., the immediate products of aromatic  
482 oxidation by OH, undergo addition of O<sub>2</sub> and NO<sub>2</sub> at comparable rates under ppm levels of NO<sub>2</sub> (rate  
483 constants of the additions of O<sub>2</sub> and NO<sub>2</sub> are on the order of 10<sup>-16</sup> and 10<sup>-11</sup> molecules cm<sup>-3</sup> s<sup>-1</sup>,  
484 respectively ;Atkinson and Arey, 2003). However, only the former addition is atmospherically relevant  
485 (Calvert et al., 2002). Liu et al. (2015) performed OFR254-iNO experiments with toluene over a range of  
486 NO<sup>in</sup> of 2.5–10 ppm, encompassing the NO concentration range at which the reactions of OH-toluene  
487 adduct with O<sub>2</sub> and with NO<sub>2</sub> are of equal importance (~5 ppm; Atkinson and Arey, 2003). This suggests  
488 that nitroaromatics, whose formation was reported in the study of Liu et al. (2015), might have been  
489 formed in substantial amounts in that study through the addition of NO<sub>2</sub> to the OH-toluene adduct.

#### 490 3.4.2 NO<sub>3</sub>

491 As discussed in Section 3.1, NO<sub>3</sub> can be formed in significant amounts in OFRs with high NO  
492 injection. Although NO<sub>3</sub> is also present in the atmosphere, especially during nighttime, significant VOC  
493 oxidation by both OH and NO<sub>3</sub> results in more complex chemistry that may complicate the  
494 interpretation of experimental results. NO<sub>3</sub> oxidation-only OFR has been previously realized  
495 experimentally via thermal dissociation of injected N<sub>2</sub>O<sub>5</sub> (Palm et al., 2017). We discuss below how to  
496 avoid significant VOC oxidation by NO<sub>3</sub> and achieve OH-dominated VOC oxidation in OFRs with high NO  
497 injection.

498 If NO<sub>3exp</sub>/OH<sub>exp</sub> > 0.1, NO<sub>3</sub> can be a competitive reactant for biogenic alkenes and dihydrofurans,  
499 which have a C=C bond for NO<sub>3</sub> addition, and phenols, which have activated hydroxyl for fast hydrogen  
500 abstraction by NO<sub>3</sub> (Atkinson and Arey, 2003), while for lower NO<sub>3exp</sub>/OH<sub>exp</sub>, OH is expected to dominate  
501 the oxidation of all VOCs, as shown in Fig. 6. Oxidation for VOCs without alkene C=C bonds and phenol  
502 hydroxyl (such as alkanes and (alkyl)benzenes) is dominated by OH unless NO<sub>3exp</sub>/OH<sub>exp</sub> > 1000. Despite  
503 its double bond, ethene reacts as slowly with NO<sub>3</sub> as alkanes, likely due to lack of alkyl groups enriching  
504 electron density on the C=C bond, which slows NO<sub>3</sub> addition. We calculate NO<sub>3exp</sub>/OH<sub>exp</sub> for OFR185-  
505 iNO and OFR254-iNO and plot histograms of this ratio in Fig. 6. Many experimental conditions lead to

506 high enough  $\text{NO}_{3\text{exp}}/\text{OH}_{\text{exp}}$  that  $\text{NO}_3$  is a competitive sink for alkenes, while only under very extreme  
507 conditions can  $\text{NO}_3$  be a competitive sink for species without C=C bonds. High-NO conditions in OFR185-  
508 iNO have lower  $\text{NO}_{3\text{exp}}/\text{OH}_{\text{exp}}$  ( $\sim 10^{-2}$ – $10^2$ ) than in OFR254-iNO ( $\sim 10^1$ – $10^5$ ) (Figs. 6 and S3d,g,j). This  
509 difference in  $\text{NO}_{3\text{exp}}/\text{OH}_{\text{exp}}$  is due to the different levels of  $\text{O}_3$  in the two modes, as high  $\text{O}_3$  promotes  
510  $\text{NO}_2$ -to- $\text{NO}_3$  oxidation. Note that low-NO conditions in both OFR185-iNO and OFR254-iNO can also reach  
511 high  $\text{NO}_{3\text{exp}}/\text{OH}_{\text{exp}}$  as some high-NO conditions have. This is because in OFR185-iNO a large part of  $\text{NO}_3$   
512 is formed by OH oxidation, resulting in  $\text{NO}_{3\text{exp}}/\text{OH}_{\text{exp}}$  being largely influenced by  $\text{NO}^{\text{in}}$  but not by other  
513 factors mainly governing OH (Fig. S3d); and under low-NO conditions in OFR254-iNO,  $\text{NO}_3$  can form  
514 rapidly from  $\text{NO}_2+\text{O}_3$ , while OH can be heavily suppressed by high  $\text{OHR}_{\text{ext}}$  (Fig. S3g,j).

515 Most of the species shown in Fig. 6 are primary VOCs, except phenols and a dihydrofuran, which  
516 can be intermediates of the atmospheric oxidation of (alkyl)benzenes (Atkinson and Arey, 2003) and  
517 long-chain alkanes (Aimanant and Ziemann, 2013; Strollo and Ziemann, 2013; Ranney and Ziemann,  
518 2016), respectively. Nevertheless, only the phenol production may occur in high-NO OFRs, as the  
519 particle-phase reaction in the photochemical formation of dihydrofurans from alkanes is too slow  
520 compared to typical OFR residence times (Ranney and Ziemann, 2016). Therefore, the impact of  $\text{NO}_3$   
521 oxidation on VOC fate needs to be considered only if the OFR input flow contains high NO mixed with  
522 biogenics and/or aromatics [(alkyl)benzenes and/or phenols]. However, (alkyl)benzenes were likely to  
523 be major SOA precursors in, to our knowledge, the only few literature OFR studies with high NO levels  
524 (Ortega et al., 2013; Tkacik et al., 2014; Liu et al., 2015). In the study of the air in a traffic tunnel (OFR185-  
525 iNO mode; Tkacik et al., 2014), where toluene is usually a major anthropogenic SOA precursor as in  
526 other urban environments (Dzepina et al., 2009; Borbon et al., 2013; Hayes et al., 2015; Jathar et al.,  
527 2015),  $\text{NO}_x$  was several hundreds of ppb. This resulted in an estimated  $\text{NO}_{3\text{exp}}/\text{OH}_{\text{exp}}$  range of  $\sim 0.1$ – $1$ ,  
528 where up to  $\sim 30\%$  of cresols (intermediates of toluene oxidation) may have been consumed by  $\text{NO}_3$ .  
529 Dihydrofurans may also have formed in the tunnel air (but outside the OFR) in the presence of  $\text{NO}_x$   
530 (Aimanant and Ziemann, 2013; Strollo and Ziemann, 2013) and, after entering the OFR, they would have  
531 been substantially (up to  $\sim 50\%$ ) consumed by  $\text{NO}_3$ . In the laboratory experiment of Liu et al. (2015) with  
532 toluene, the injection of as much as 10 ppm NO elevated  $\text{NO}_{3\text{exp}}/\text{OH}_{\text{exp}}$  to  $\sim 100$ , where cresols from  
533 toluene oxidation reacted almost exclusively with  $\text{NO}_3$  in addition to being photolyzed.

#### 534 3.4.3 A case study

535 We use a case study of an OFR254-13-iNO laboratory experiment with a large amount of toluene  
536 (5 ppm) and  $\text{NO}^{\text{in}}$  (10 ppm) to illustrate how very high VOC and NO concentrations cause multiple types  
537 of atmospherically irrelevant reactions in OFR. Due to very high  $\text{OHR}_{\text{ext}}$  and  $\text{NO}^{\text{in}}$ , photolysis of toluene  
538 at 254 nm may have been important (Peng et al., 2016). In case of a high (close to 1) quantum yield, up  
539 to  $\sim 80\%$  of the consumed toluene in their experiments could have been photolyzed (Scheme 1). Of the  
540 rest of reacted toluene,  $\sim 10\%$  undergoes H-abstraction by OH from the methyl group in the model,  
541 leading to an  $\text{RO}_2$  similar to alkyl  $\text{RO}_2$  and likely proceeding with normal  $\text{RO}_2$  chemistry.  $\sim 90\%$  of the  
542 toluene formed an OH-adduct (Calvert et al., 2002). As discussed above, 70% of this adduct (depending  
543 on  $\text{NO}^{\text{in}}$ ) is predicted to recombine with  $\text{NO}_2$  producing nitroaromatics because of the ppm-level  $\text{NO}_x$ .

544 The adduct could also react with O<sub>2</sub> via two types of pathways, of which one was addition forming a  
545 special category of RO<sub>2</sub> (OH-toluene-O<sub>2</sub> adducts) potentially undergoing ring-opening (Atkinson and  
546 Arey, 2003; Orlando and Tyndall, 2012; Ziemann and Atkinson, 2012), the other H-elimination by O<sub>2</sub>  
547 producing cresols. Again, like toluene, cresols may have been substantially photolyzed. As a result of  
548 NO<sub>3exp</sub>/OH<sub>exp</sub> ~100, only a minor portion of cresol could have undergone OH addition and then H-  
549 elimination again. This pathway leads to the formation of methylidihydroxybenzenes and other OH-  
550 oxidation products (Atkinson and Arey, 2003). The rest of cresols may have formed methylphenoxy  
551 radicals, nevertheless, dominantly via H-abstraction by NO<sub>3</sub>, since H-abstraction by OH was even a minor  
552 pathway compared to the OH-addition one (Atkinson et al., 1992). In summary, the model results  
553 suggest that there were two possible routes leading to nitroaromatic formation. However, one of them  
554 (recombination of OH-aromatic adducts with NO<sub>2</sub>) is likely of little atmospheric relevance due to very  
555 high NO<sub>x</sub> needed, and the other (H-abstraction from cresol) occurs in the atmosphere but is not a major  
556 fate of aromatics (Calvert et al., 2002).

### 557 3.5 Implications for OFR experiments with combustion emissions as input

558 Emissions from combustion sources, e.g., vehicles and biomass burning, usually contain VOCs  
559 and NO<sub>x</sub> at very high concentrations (Table 1). An injection of this type of emissions (typically with OHR<sub>ext</sub>  
560 of thousands of s<sup>-1</sup> or larger and NO<sup>in</sup> of tens of ppm or larger) in OFRs without any pretreatment is likely  
561 to cause all experimental issues discussed in Peng et al. (2016) and this paper, i.e., strong OH  
562 suppression, substantial non-tropospheric photolysis, strong RO<sub>2</sub> suppression by NO<sub>2</sub> whether RO<sub>2</sub> is  
563 acyl RO<sub>2</sub> or not, fast reactions of NO<sub>2</sub> with OH-aromatic hydrocarbon adducts, substantial NO<sub>3</sub>  
564 contribution to VOC fate, and even a near-total inhibition of OFR chemistry due to complete titration of  
565 O<sub>3</sub> by NO in the case of OFR254. We take the study of Karjalainen et al. (2016), who used an OFR to  
566 oxidize diluted car exhaust in real-time, as a case study to investigate the extent to which these issues  
567 may affect typical combustion source studies and to explore approaches to mitigate the problems.

568 During the first 200 s of their experiment (defined as the “cold start” period when the catalyst is  
569 cold and emissions are high), NO and total hydrocarbon in the emissions of the test vehicle reached  
570 ~400 and ~600 ppm, respectively. We first simulate the oxidation of those emissions without any  
571 dilution (even though x12 dilution was used in their experiments) to explore the most extreme  
572 conditions. Our model simulation indicates that such an extremely concentrated source would generally  
573 lead to bad high- or low-NO conditions (depending on NO concentration) in their OFR (Fig. 7), even  
574 though it was run at relatively high H<sub>2</sub>O and UV. OH suppression can be as high as 3 orders of magnitude;  
575 VOC fates by non-tropospheric photolysis and reactions of alkenes and phenols with NO<sub>3</sub> can be nearly  
576 100%; up to ~1/3 of OH-toluene adduct may be recombined with NO<sub>2</sub> instead of forming an adduct with  
577 O<sub>2</sub>. After the test vehicle entered the “hot stabilized” stage (200–1000 s), its VOC emissions (on the  
578 order of ppm) were still too high for an undiluted OFR to yield a good condition (Fig. S9). OH suppression  
579 can still reach 2 orders of magnitude; non-tropospheric photolysis, and sometimes reactions with NO<sub>3</sub>,  
580 can still dominate over reactions with OH in VOC fates; reactions of OH-toluene adduct with NO<sub>2</sub> can  
581 still be substantial at some small NO emission spikes. Moreover, although NO emissions were roughly

582 at ppm level even during the hot stabilized period, NO effective lifetime may be very short during that  
583 period, leading to low-NO conditions in their OFR.

584 As suggested in Peng et al. (2016) for low-NO OFR, dilution of sources can also mitigate strong  
585 deviations on OFR-iNO chemistry vs. atmospherically-relevant conditions. A dilution by a factor of 12,  
586 as actually used by Karjalainen et al. (2016), appears to be sufficient to bring most of the hot stabilized  
587 period under good conditions (Fig. S9). However, most VOC, or in other words, most SOA formation  
588 potential, was emitted during the cold start period, when risky and bad conditions still prevailed (Figs.  
589 7 and 8). Even if the emissions are diluted by x100, the cold-start emission peak (Fig. 7) is still under  
590 risky conditions. Although bad conditions are eliminated and good condition is present during most of  
591 time, this emission peak under risky condition may contribute >50% to total SOA formation potential  
592 (Fig. 8). For SOA formed under good condition to be dominant, a dilution factor >400 would be needed.

593 Note that a strong dilution lowers aerosol mass loading in vehicle emissions. As a result, condensation  
594 of gases onto particles is slower than in raw exhausts. However, condensational sinks after dilution may  
595 still be significantly higher than typical ambient values (Matti Maricq, 2007; Donahue et al., 2016).

596 Note that the emissions of the test vehicle of Karjalainen et al. (2016) are rather clean compared  
597 to the typical 2013 US on-road fleet (i.e., all at the hot stabilized stage) measured by Bishop and  
598 Stedman (2013) (Figs. 9 and S10). For emissions of an average on-road fleet, a dilution by a factor of  
599 100 or larger would be necessary to ensure that most emissions would be processed in OFR185 under  
600 good conditions at the highest H<sub>2</sub>O and UV in this study (Figs. 9b and S10b,e,h). In the case of lower H<sub>2</sub>O  
601 and/or UV, an even larger dilution factor would be required.

602 Conducting OFR185-iNO experiments at high UV lowers the dilution factor needed for good  
603 conditions. However, it also renders good high-NO condition impossible (see Section 3.2 and Fig. S4). If  
604 one wants to oxidize vehicle exhausts in a high-NO environment in OFR, as in an urban atmosphere,  
605 OFR185 at low UV is necessary. Consequently, a much stronger dilution is in turn necessary to keep the  
606 operation condition still good. Nevertheless, not all vehicle emissions can be moved into good high-NO  
607 region through a simple dilution (Figs. 9c and S10c,f,i). Furthermore, a low UV would seriously limit the  
608 highest OH<sub>exp</sub> that OFR can achieve ( $\sim 3 \times 10^{11}$  molecules cm<sup>-3</sup> s for modeled good high-NO conditions in  
609 this study), while a much higher OH<sub>exp</sub> would be desirable to fully convert SOA formation potential into  
610 measurable SOA mass. If both good high-NO condition and high OH<sub>exp</sub> are required, new techniques  
611 (e.g., injection of N<sub>2</sub>O at percent level proposed by Lambe et al. (2017)) may be necessary.

#### 612 **4 Conclusions**

613 In this study, OFR chemistry involving NO<sub>y</sub> species was systematically investigated over a wide  
614 range of conditions. NO initially injected into the OFR was found to be rapidly oxidized under most  
615 conditions. In particular, due to high O<sub>3</sub> concentrations, NO lifetime in OFR254-iNO was too short to  
616 result in a significant RO<sub>2</sub> consumption by NO compared to that by HO<sub>2</sub> under all conditions with active  
617 chemistry. Nevertheless, it is not completely impossible for OFR185-iNO to have a significant RO<sub>2</sub> fate  
618 by NO and minor non-tropospheric photolysis at the same time ("good high-NO conditions"). According  
619 to our simulations, these conditions are most likely present at high H<sub>2</sub>O, low UV, low OHR<sub>ext</sub>, and NO<sup>in</sup>

620 of tens to hundreds of ppb.

621         However, many past OFR studies with high NO injection were conducted under conditions  
622 remarkably different from the abovementioned very narrow range.  $\text{NO}^{\text{th}}$  and/or  $\text{OHR}_{\text{ext}}$  in those studies  
623 were often much higher than good high-NO conditions require (particularly, >3 orders of magnitude in  
624 some OFR studies using combustion emissions as input). In addition to non-tropospheric organic  
625 photolysis, OFR oxidation of highly concentrated sources can cause multiple large deviations from  
626 tropospheric OH oxidation, i.e.,  $\text{RO}_2$  suppression by high  $\text{NO}_2$ , substantial nitroaromatic formation from  
627 the recombination of  $\text{NO}_2$  and OH-aromatic adducts, and fast reactions of VOCs with  $\text{NO}_3$  compared to  
628 those with OH.

629         Working at lower  $\text{NO}_x$  (sub-ppm level) and VOC concentrations or dilution can mitigate these  
630 experimental problems. In general, a strong dilution (by a factor of >100) is needed for OFR that process  
631 typical on-road vehicle emissions. Humidification can also make good conditions more likely. By these  
632 measures, good conditions can be guaranteed, as long as NO and/or precursor concentrations are  
633 sufficiently low, while high-NO conditions cannot be ensured. To aid design and interpretation of OFR  
634 experiments with high NO injection, we provide our detailed modeling results in a visualized form (Fig.  
635 S3). For OFR users in need for both high  $\text{OH}_{\text{exp}}$  and high NO, simple NO injection is not a good option.  
636 New techniques (e.g., injection of  $\text{N}_2\text{O}$  proposed by Lambe et al. (2017) or other innovations) may be  
637 necessary to meet this need.

638

639

#### 640 **Acknowledgements**

641 This work was partially supported by DOE (BER/ASR) DE-SC0011105 & DE-SC0016559, EPA STAR  
642 83587701-0, and NSF AGS-1360834. We thank Pengfei Liu, Andrew Lambe, and Daniel Tkacik for  
643 providing some OFR experimental data, the authors of Karjalainen et al. (2016) and their project IEA-  
644 AMF Annex 44 for providing the data and information for the vehicle tests, Gary Bishop for providing  
645 on-road vehicle emission data, and Andrew Lambe and William Brune for useful discussions.  
646

647 **References**

- 648 Aimanant, S. and Ziemann, P. J.: Chemical Mechanisms of Aging of Aerosol Formed from the Reaction  
649 of n-Pentadecane with OH Radicals in the Presence of NO<sub>x</sub>, *Aerosol Sci. Technol.*, 47(9), 979–990,  
650 doi:10.1080/02786826.2013.804621, 2013.
- 651 Alanen, J., Simonen, P., Saarikoski, S., Timonen, H., Kangasniemi, O., Saukko, E., Hillamo, R., Lehtoranta,  
652 K., Murtonen, T., Vesala, H., Keskinen, J. and Rönkkö, T.: Comparison of primary and secondary particle  
653 formation from natural gas engine exhaust and of their volatility characteristics, *Atmos. Chem. Phys.*  
654 *Discuss.*, (February), 1–27, doi:10.5194/acp-2017-44, 2017.
- 655 Ammann, M., Cox, R. A., Crowley, J. N., Jenkin, M. E., Mellouki, A., Rossi, M. J., Troe, J., Wallington, T. J.,  
656 Cox, B., Atkinson, R., Baulch, D. L. and Kerr, J. A.: IUPAC Task Group on Atmospheric Chemical Kinetic  
657 Data Evaluation, [online] Available from: <http://iupac.pole-ether.fr/#>, 2016.
- 658 Atkinson, R. and Arey, J.: Atmospheric degradation of volatile organic compounds., *Chem. Rev.*, 103(12),  
659 4605–38, doi:10.1021/cr0206420, 2003.
- 660 Atkinson, R., Aschmann, S. M. and Arey, J.: Reactions of hydroxyl and nitrogen trioxide radicals with  
661 phenol, cresols, and 2-nitrophenol at 296 ± 2 K, *Environ. Sci. Technol.*, 26(7), 1397–1403,  
662 doi:10.1021/es00031a018, 1992.
- 663 BIPM, IEC, IFCC, ILAC, ISO, IUPAC and IUPAPOIML: JCGM 101: 2008 Evaluation of measurement data —  
664 Supplement 1 to the “ Guide to the expression of uncertainty in measurement ” — Propagation of  
665 distributions using a Monte Carlo method., 2008.
- 666 Bishop, G. A. and Stedman, D. H.: Fuel Efficiency Automobile Test: Light-Duty Vehicles, [online] Available  
667 from: [http://www.feat.biochem.du.edu/light\\_duty\\_vehicles.html](http://www.feat.biochem.du.edu/light_duty_vehicles.html) (Accessed 1 February 2017), 2013.
- 668 Borbon, A., Gilman, J. B., Kuster, W. C., Grand, N., Chevaillier, S., Colomb, A., Dolgorouky, C., Gros, V.,  
669 Lopez, M., Sarda-Esteve, R., Holloway, J., Stutz, J., Petetin, H., McKeen, S., Beekmann, M., Warneke, C.,  
670 Parrish, D. D. and De Gouw, J. A.: Emission ratios of anthropogenic volatile organic compounds in  
671 northern mid-latitude megacities: Observations versus emission inventories in Los Angeles and Paris, *J.*  
672 *Geophys. Res. Atmos.*, 118(4), 2041–2057, doi:10.1002/jgrd.50059, 2013.
- 673 Burkholder, J. B., Sander, S. P., Abbatt, J., Barker, J. R., Huie, R. E., Kolb, C. E., Kurylo, M. J., Orkin, V. L.,  
674 Wilmouth, D. M. and Wine, P. H.: Chemical Kinetics and Photochemical Data for Use in Atmospheric  
675 Studies: Evaluation Number 18, Pasadena, CA, USA. [online] Available from:  
676 <http://jpldataeval.jpl.nasa.gov/>, 2015.
- 677 Calvert, J. G., Atkinson, R., Becker, K. H., Kamens, R. M., Seinfeld, J. H., Wallington, T. H. and Yarwood,  
678 G.: The Mechanisms of Atmospheric Oxidation of the Aromatic Hydrocarbons, Oxford University Press,  
679 USA. [online] Available from: <https://books.google.com/books?id=P0basaLrxDMC>, 2002.
- 680 Carlton, A. G., Wiedinmyer, C. and Kroll, J. H.: A review of Secondary Organic Aerosol (SOA) formation  
681 from isoprene, *Atmos. Chem. Phys.*, 9(14), 4987–5005, doi:10.5194/acp-9-4987-2009, 2009.
- 682 Carter, W. P. L., Cocker, D. R., Fitz, D. R., Malkina, I. L., Bumiller, K., Sauer, C. G., Pisano, J. T., Bufalino, C.  
683 and Song, C.: A new environmental chamber for evaluation of gas-phase chemical mechanisms and  
684 secondary aerosol formation, *Atmos. Environ.*, 39(40), 7768–7788,  
685 doi:10.1016/j.atmosenv.2005.08.040, 2005.
- 686 Chameides, W., Lindsay, R., Richardson, J. and Kiang, C.: The role of biogenic hydrocarbons in urban  
687 photochemical smog: Atlanta as a case study, *Science* (80-. ), 241(4872), 1473–1475,  
688 doi:10.1126/science.3420404, 1988.
- 689 Cocker, D. R., Flagan, R. C. and Seinfeld, J. H.: State-of-the-Art Chamber Facility for Studying Atmospheric  
690 Aerosol Chemistry, *Environ. Sci. Technol.*, 35(12), 2594–2601, doi:10.1021/es0019169, 2001.
- 691 Donahue, N. M., Posner, L. N., Westervelt, D. M., Li, Z., Shrivastava, M., Presto, A. A., Sullivan, R. C.,  
692 Adams, P. J., Pandis, S. N. and Robinson, A. L.: Where Did This Particle Come From? Sources of Particle  
693 Number and Mass for Human Exposure Estimates, in *Airborne Particulate Matter: Sources, Atmospheric*  
694 *Processes and Health*, edited by R. M. Harrison, R. E. Hester, and X. Querol, pp. 35–71, Royal Society of  
695 Chemistry, 2016.
- 696 Dzepina, K., Volkamer, R. M., Madronich, S., Tulet, P., Ulbrich, I. M., Zhang, Q., Cappa, C. D., Ziemann, P.



697 J. and Jimenez, J. L.: Evaluation of recently-proposed secondary organic aerosol models for a case study  
698 in Mexico City, *Atmos. Chem. Phys.*, 9(15), 5681–5709, doi:10.5194/acp-9-5681-2009, 2009.

699 George, I. J., Vlasenko, A., Slowik, J. G., Broekhuizen, K. and Abbatt, J. P. D.: Heterogeneous oxidation of  
700 saturated organic aerosols by hydroxyl radicals: uptake kinetics, condensed-phase products, and particle  
701 size change, *Atmos. Chem. Phys.*, 7(16), 4187–4201, doi:10.5194/acp-7-4187-2007, 2007.

702 Haagen-Smit, A. J.: Chemistry and Physiology of Los Angeles Smog, *Ind. Eng. Chem.*, 44(6), 1342–1346,  
703 doi:10.1021/ie50510a045, 1952.

704 Hallquist, M., Wenger, J. C., Baltensperger, U., Rudich, Y., Simpson, D., Claeys, M., Dommen, J., Donahue,  
705 N. M., George, C., Goldstein, A. H., Hamilton, J. F., Herrmann, H., Hoffmann, T., Iinuma, Y., Jang, M.,  
706 Jenkin, M. E., Jimenez, J. L., Kiendler-Scharr, A., Maenhaut, W., McFiggans, G., Mentel, T. F., Monod, A.,  
707 Prevot, A. S. H., Seinfeld, J. H., Surratt, J. D., Szmigielski, R. and Wildt, J.: The formation, properties and  
708 impact of secondary organic aerosol: current and emerging issues, *Atmos. Chem. Phys.*, 9(14), 5155–  
709 5236, 2009.

710 Hayes, P. L., Carlton, a. G., Baker, K. R., Ahmadov, R., Washenfelder, R. a., Alvarez, S., Rappenglück, B.,  
711 Gilman, J. B., Kuster, W. C., de Gouw, J. a., Zotter, P., Prévôt, a. S. H., Szidat, S., Kleindienst, T. E., Offenberg,  
712 J. H., Ma, P. K. and Jimenez, J. L.: Modeling the formation and aging of secondary organic aerosols in Los  
713 Angeles during CalNex 2010, *Atmos. Chem. Phys.*, 15(10), 5773–5801, doi:10.5194/acp-15-5773-2015,  
714 2015.

715 Hearn, J. D. and Smith, G. D.: Kinetics and Product Studies for Ozonolysis Reactions of Organic Particles  
716 Using Aerosol CIMS †, *J. Phys. Chem. A*, 108(45), 10019–10029, doi:10.1021/jp0404145, 2004.

717 Hoffmann, T., Odum, J. R., Bowman, F., Collins, D., Klockow, D., Flagan, R. C. and Seinfeld, J. H.:  
718 Formation of Organic Aerosols from the Oxidation of Biogenic Hydrocarbons, *J. Atmos. Chem.*, 26(2),  
719 189–222, doi:10.1023/A:1005734301837, 1997.

720 Hu, W., Palm, B. B., Day, D. A., Campuzano-Jost, P., Krechmer, J. E., Peng, Z., de Sá, S. S., Martin, S. T.,  
721 Alexander, M. L., Baumann, K., Hacker, L., Kiendler-Scharr, A., Koss, A. R., de Gouw, J. A., Goldstein, A.  
722 H., Seco, R., Sjöstedt, S. J., Park, J.-H., Guenther, A. B., Kim, S., Canonaco, F., Prévôt, A. S. H., Brune, W.  
723 H. and Jimenez, J. L.: Volatility and lifetime against OH heterogeneous reaction of ambient isoprene-  
724 epoxydiols-derived secondary organic aerosol (IEPOX-SOA), *Atmos. Chem. Phys.*, 16(18), 11563–11580,  
725 doi:10.5194/acp-16-11563-2016, 2016.

726 Jathar, S. H., Cappa, C. D., Wexler, a. S., Seinfeld, J. H. and Kleeman, M. J.: Multi-generational oxidation  
727 model to simulate secondary organic aerosol in a 3-D air quality model, *Geosci. Model Dev.*, 8(8), 2553–  
728 2567, doi:10.5194/gmd-8-2553-2015, 2015.

729 Kang, E., Root, M. J., Toohey, D. W. and Brune, W. H.: Introducing the concept of Potential Aerosol Mass  
730 (PAM), *Atmos. Chem. Phys.*, 7(22), 5727–5744, doi:10.5194/acp-7-5727-2007, 2007.

731 Kang, E., Toohey, D. W. and Brune, W. H.: Dependence of SOA oxidation on organic aerosol mass  
732 concentration and OH exposure: experimental PAM chamber studies, *Atmos. Chem. Phys.*, 11(4), 1837–  
733 1852, doi:10.5194/acp-11-1837-2011, 2011.

734 Karjalainen, P., Timonen, H., Saukko, E., Kuuluvainen, H., Saarikoski, S., Aakko-Saksa, P., Murtonen, T.,  
735 Bloss, M., Dal Maso, M., Simonen, P., Ahlberg, E., Svenningsson, B., Brune, W. H., Hillamo, R., Keskinen,  
736 J. and Rönkkö, T.: Time-resolved characterization of primary particle emissions and secondary particle  
737 formation from a modern gasoline passenger car, *Atmos. Chem. Phys.*, 16(13), 8559–8570,  
738 doi:10.5194/acp-16-8559-2016, 2016.

739 Krechmer, J. E., Pagonis, D., Ziemann, P. J. and Jimenez, J. L.: Quantification of Gas-Wall Partitioning in  
740 Teflon Environmental Chambers Using Rapid Bursts of Low-Volatility Oxidized Species Generated in Situ,  
741 *Environ. Sci. Technol.*, 50(11), 5757–5765, doi:10.1021/acs.est.6b00606, 2016.

742 Lakey, P. S. J., George, I. J., Whalley, L. K., Baeza-Romero, M. T. and Heard, D. E.: Measurements of the  
743 HO<sub>2</sub> Uptake Coefficients onto Single Component Organic Aerosols, *Environ. Sci. Technol.*, 49(8), 4878–  
744 4885, doi:10.1021/acs.est.5b00948, 2015.

745 Lambe, A., Massoli, P., Zhang, X., Canagaratna, M., Nowak, J., Daube, C., Yan, C., Nie, W., Onasch, T.,  
746 Jayne, J., Kolb, C., Davidovits, P., Worsnop, D. and Brune, W.: Controlled nitric oxide production via  
747 O(<sup>1</sup>S) + N<sub>2</sub>O → NO + O<sub>2</sub> + N<sub>2</sub>, *Environ. Sci. Technol.*, 50(11), 5757–5765, doi:10.1021/acs.est.6b00606, 2016.

748 reactions for use in oxidation flow reactor studies, *Atmos. Meas. Tech.*, 10(6), 2283–2298,  
749 doi:10.5194/amt-10-2283-2017, 2017.

750 Lambe, A. T., Ahern, A. T., Williams, L. R., Slowik, J. G., Wong, J. P. S., Abbatt, J. P. D., Brune, W. H., Ng, N.  
751 L., Wright, J. P., Croasdale, D. R., Worsnop, D. R., Davidovits, P. and Onasch, T. B.: Characterization of  
752 aerosol photooxidation flow reactors: heterogeneous oxidation, secondary organic aerosol formation  
753 and cloud condensation nuclei activity measurements, *Atmos. Meas. Tech.*, 4(3), 445–461,  
754 doi:10.5194/amt-4-445-2011, 2011.

755 Lambe, A. T. and Jimenez, J. L.: PAM Wiki: Publications Using the PAM Oxidation Flow Reactor, [online]  
756 Available from: <https://sites.google.com/site/pamwiki/publications> (Accessed 10 February 2017), 2017.

757 Levy II, H.: Normal atmosphere: large radical and formaldehyde concentrations predicted., *Science*,  
758 173(3992), 141–143, doi:10.1126/science.173.3992.141, 1971.

759 Li, R., Palm, B. B., Borbon, A., Graus, M., Warneke, C., Ortega, a M., Day, D. a, Brune, W. H., Jimenez, J.  
760 L. and de Gouw, J. a: Laboratory Studies on Secondary Organic Aerosol Formation from Crude Oil Vapors,  
761 *Environ. Sci. Technol.*, 47(21), 12566–12574, doi:10.1021/es402265y, 2013.

762 Li, R., Palm, B. B., Ortega, A. M., Hu, W., Peng, Z., Day, D. A., Knote, C., Brune, W. H., de Gouw, J. and  
763 Jimenez, J. L.: Modeling the radical chemistry in an Oxidation Flow Reactor (OFR): radical formation and  
764 recycling, sensitivities, and OH exposure estimation equation, *J. Phys. Chem. A*, 119(19), 4418–4432,  
765 doi:10.1021/jp509534k, 2015.

766 Link, M. F., Friedman, B., Fulgham, R., Brophy, P., Galang, A., Jathar, S. H., Veres, P., Roberts, J. M. and  
767 Farmer, D. K.: Photochemical processing of diesel fuel emissions as a large secondary source of isocyanic  
768 acid (HNCO), *Geophys. Res. Lett.*, 43(8), 4033–4041, doi:10.1002/2016GL068207, 2016.

769 Lippmann, M.: Health effects of tropospheric ozone, *Environ. Sci. Technol.*, 25(12), 1954–1962,  
770 doi:10.1021/es00024a001, 1991.

771 Liu, P. F., Abdelmalki, N., Hung, H.-M., Wang, Y., Brune, W. H. and Martin, S. T.: Ultraviolet and visible  
772 complex refractive indices of secondary organic material produced by photooxidation of the aromatic  
773 compounds toluene and m-Xylene, *Atmos. Chem. Phys.*, 15(3), 1435–1446, doi:10.5194/acp-15-1435-  
774 2015, 2015.

775 Mao, J., Ren, X., Brune, W. H., Olson, J. R., Crawford, J. H., Fried, a., Huey, L. G., Cohen, R. C., Heikes, B.,  
776 Singh, H. B., Blake, D. R., Sachse, G. W., Diskin, G. S., Hall, S. R. and Shetter, R. E.: Airborne measurement  
777 of OH reactivity during INTEX-B, *Atmos. Chem. Phys.*, 9(1), 163–173, doi:10.5194/acp-9-163-2009, 2009.

778 Martinsson, J., Eriksson, A. C., Nielsen, I. E., Malmberg, V. B., Ahlberg, E., Andersen, C., Lindgren, R.,  
779 Nyström, R., Nordin, E. Z., Brune, W. H., Svenningsson, B., Swietlicki, E., Boman, C. and Pagels, J. H.:  
780 Impacts of Combustion Conditions and Photochemical Processing on the Light Absorption of Biomass  
781 Combustion Aerosol, *Environ. Sci. Technol.*, 49(24), 14663–14671, doi:10.1021/acs.est.5b03205, 2015.

782 Matsunaga, A. and Ziemann, P. J.: Gas-Wall Partitioning of Organic Compounds in a Teflon Film Chamber  
783 and Potential Effects on Reaction Product and Aerosol Yield Measurements, *Aerosol Sci. Technol.*, 44(10),  
784 881–892, doi:10.1080/02786826.2010.501044, 2010.

785 Moise, T. and Rudich, Y.: Reactive Uptake of Ozone by Aerosol-Associated Unsaturated Fatty Acids:  
786 Kinetics, Mechanism, and Products, *J. Phys. Chem. A*, 106(27), 6469–6476, doi:10.1021/jp025597e,  
787 2002.

788 Moise, T., Talukdar, R. K., Frost, G. J., Fox, R. W. and Rudich, Y.: Reactive uptake of NO<sub>3</sub> by liquid and  
789 frozen organics, *J. Geophys. Res.*, 107(D2), 4014, doi:10.1029/2001JD000334, 2002.

790 Nehr, S., Bohn, B., Fuchs, H., Häseler, R., Hofzumahaus, A., Li, X., Rohrer, F., Tillmann, R. and Wahner, A.:  
791 Atmospheric photochemistry of aromatic hydrocarbons: OH budgets during SAPHIR chamber  
792 experiments, *Atmos. Chem. Phys.*, 14(13), 6941–6952, doi:10.5194/acp-14-6941-2014, 2014.

793 Nel, A.: Air Pollution-Related Illness: Effects of Particles, *Science (80-. )*, 308(5723), 804–806,  
794 doi:10.1126/science.1108752, 2005.

795 Ng, N. L., Canagaratna, M. R., Zhang, Q., Jimenez, J. L., Tian, J., Ulbrich, I. M., Kroll, J. H., Docherty, K. S.,  
796 Chhabra, P. S., Bahreini, R., Murphy, S. M., Seinfeld, J. H., Hildebrandt, L., Donahue, N. M., DeCarlo, P. F.,  
797 Lanz, V. a., Prévôt, a. S. H., Dinar, E., Rudich, Y., Worsnop, D. R., Prevot, A. S. H., Dinar, E., Rudich, Y. and

798 Worsnop, D. R.: Organic aerosol components observed in Northern Hemispheric datasets from Aerosol  
799 Mass Spectrometry, *Atmos. Chem. Phys.*, 10(10), 4625–4641, doi:10.5194/acp-10-4625-2010, 2010.

800 Odum, J. R., Hoffmann, T., Bowman, F., Collins, D., Flagan Richard, C. and Seinfeld John, H.: Gas particle  
801 partitioning and secondary organic aerosol yields, *Environ. Sci. Technol.*, 30(8), 2580–2585,  
802 doi:10.1021/es950943+, 1996.

803 Orlando, J. J. and Tyndall, G. S.: Laboratory studies of organic peroxy radical chemistry: an overview with  
804 emphasis on recent issues of atmospheric significance, *Chem. Soc. Rev.*, 41(19), 6294,  
805 doi:10.1039/c2cs35166h, 2012.

806 Ortega, A. M., Day, D. A., Cubison, M. J., Brune, W. H., Bon, D., de Gouw, J. A. and Jimenez, J. L.:  
807 Secondary organic aerosol formation and primary organic aerosol oxidation from biomass-burning  
808 smoke in a flow reactor during FLAME-3, *Atmos. Chem. Phys.*, 13(22), 11551–11571, doi:10.5194/acp-  
809 13-11551-2013, 2013.

810 Ortega, A. M., Hayes, P. L., Peng, Z., Palm, B. B., Hu, W., Day, D. A., Li, R., Cubison, M. J., Brune, W. H.,  
811 Graus, M., Warneke, C., Gilman, J. B., Kuster, W. C., de Gouw, J., Gutiérrez-Montes, C. and Jimenez, J. L.:  
812 Real-time measurements of secondary organic aerosol formation and aging from ambient air in an  
813 oxidation flow reactor in the Los Angeles area, *Atmos. Chem. Phys.*, 16(11), 7411–7433,  
814 doi:10.5194/acp-16-7411-2016, 2016.

815 Palm, B. B., Campuzano-Jost, P., Day, D. A., Ortega, A. M., Fry, J. L., Brown, S. S., Zarzana, K. J., Dube, W.,  
816 Wagner, N. L., Draper, D. C., Kaser, L., Jud, W., Karl, T., Hansel, A., Gutiérrez-Montes, C. and Jimenez, J.  
817 L.: Secondary organic aerosol formation from in situ OH, O<sub>3</sub>, and NO<sub>3</sub> oxidation of ambient forest air in  
818 an oxidation flow reactor, *Atmos. Chem. Phys.*, 17(8), 5331–5354, doi:10.5194/acp-17-5331-2017, 2017.

819 Palm, B. B., Campuzano-Jost, P., Ortega, A. M., Day, D. A., Kaser, L., Jud, W., Karl, T., Hansel, A., Hunter, J.  
820 F., Cross, E. S., Kroll, J. H., Peng, Z., Brune, W. H. and Jimenez, J. L.: In situ secondary organic aerosol  
821 formation from ambient pine forest air using an oxidation flow reactor, *Atmos. Chem. Phys.*, 16(5),  
822 2943–2970, doi:10.5194/acp-16-2943-2016, 2016.

823 Peng, Z., Carrasco, N. and Pernet, P.: Modeling of synchrotron-based laboratory simulations of Titan's  
824 ionospheric photochemistry, *GeoResJ*, 1–2, 33–53, doi:10.1016/j.grj.2014.03.002, 2014.

825 Peng, Z., Day, D. A., Ortega, A. M., Palm, B. B., Hu, W., Stark, H., Li, R., Tsigaridis, K., Brune, W. H. and  
826 Jimenez, J. L.: Non-OH chemistry in oxidation flow reactors for the study of atmospheric chemistry  
827 systematically examined by modeling, *Atmos. Chem. Phys.*, 16(7), 4283–4305, doi:10.5194/acp-16-  
828 4283-2016, 2016.

829 Peng, Z., Day, D. A., Stark, H., Li, R., Lee-Taylor, J., Palm, B. B., Brune, W. H. and Jimenez, J. L.: HOx radical  
830 chemistry in oxidation flow reactors with low-pressure mercury lamps systematically examined by  
831 modeling, *Atmos. Meas. Tech.*, 8(11), 4863–4890, doi:10.5194/amt-8-4863-2015, 2015.

832 Ranney, A. P. and Ziemann, P. J.: Kinetics of Acid-Catalyzed Dehydration of Cyclic Hemiacetals in Organic  
833 Aerosol Particles in Equilibrium with Nitric Acid Vapor, *J. Phys. Chem. A*, 120(16), 2561–2568,  
834 doi:10.1021/acs.jpca.6b01402, 2016.

835 Richards-Henderson, N. K., Goldstein, A. H. and Wilson, K. R.: Large Enhancement in the Heterogeneous  
836 Oxidation Rate of Organic Aerosols by Hydroxyl Radicals in the Presence of Nitric Oxide, *J. Phys. Chem.*  
837 *Let.*, 6, 4451–4455, doi:10.1021/acs.jpcl.5b02121, 2015.

838 Saltelli, A., Ratto, M., Tarantola, S. and Campolongo, F.: Sensitivity Analysis for Chemical Models, *Chem.*  
839 *Rev.*, 105(7), 2811–2828, doi:10.1021/cr040659d, 2005.

840 Sander, S. P., Friedl, R. R., Barker, J. R., Golden, D. M., Kurylo, M. J., Wine, P. H., Abbatt, J. P. D., Burkholder,  
841 J. B., Kolb, C. E., Moortgat, G. K., Huie, R. E. and Orkin, V. L.: Chemical Kinetics and Photochemical Data  
842 for Use in Atmospheric Studies Evaluation Number 17, Pasadena, CA, USA. [online] Available from:  
843 [http://jpldataeval.jpl.nasa.gov/pdf/JPL\\_10-6\\_Final\\_15June2011.pdf](http://jpldataeval.jpl.nasa.gov/pdf/JPL_10-6_Final_15June2011.pdf), 2011.

844 Schill, G. P., Jathar, S. H., Kodros, J. K., Levin, E. J. T., Galang, A. M., Friedman, B., Link, M. F., Farmer, D.  
845 K., Pierce, J. R., Kreidenweis, S. M. and DeMott, P. J.: Ice-nucleating particle emissions from  
846 photochemically aged diesel and biodiesel exhaust, *Geophys. Res. Lett.*, 43(10), 5524–5531,  
847 doi:10.1002/2016GL069529, 2016.

848 Schwantes, R. H., Schilling, K. A., McVay, R. C., Lignell, H., Coggon, M. M., Zhang, X., Wennberg, P. O. and

849 Seinfeld, J. H.: Formation of highly oxygenated low-volatility products from cresol oxidation, *Atmos.*  
850 *Chem. Phys.*, 17(5), 3453–3474, doi:10.5194/acp-17-3453-2017, 2017.

851 Seakins, P. W.: A brief review of the use of environmental chambers for gas phase studies of kinetics,  
852 chemical mechanisms and characterisation of field instruments, *EPJ Web Conf.*, 9, 143–163,  
853 doi:10.1051/epjconf/201009012, 2010.

854 Simonen, P., Saukko, E., Karjalainen, P., Timonen, H., Bloss, M., Aakko-Saksa, P., Rönkkö, T., Keskinen, J.  
855 and Dal Maso, M.: A new oxidation flow reactor for measuring secondary aerosol formation of rapidly  
856 changing emission sources, *Atmos. Meas. Tech.*, 10(4), 1519–1537, doi:10.5194/amt-10-1519-2017,  
857 2017.

858 Stocker, T. F., Qin, D., Plattner, G.-K., Tignor, M., Allen, S. K., Boschung, J., Nauels, A., Xia, Y., Bex, V. and  
859 Midgley, P. M.: *Climate Change 2013 - The Physical Science Basis*, edited by Intergovernmental Panel on  
860 Climate Change, Cambridge University Press, Cambridge., 2014.

861 Strollo, C. M. and Ziemann, P. J.: Products and mechanism of secondary organic aerosol formation from  
862 the reaction of 3-methylfuran with OH radicals in the presence of NO<sub>x</sub>, *Atmos. Environ.*, 77, 534–543,  
863 doi:10.1016/j.atmosenv.2013.05.033, 2013.

864 Tkacik, D. S., Lambe, A. T., Jathar, S., Li, X., Presto, A. A., Zhao, Y., Blake, D., Meinardi, S., Jayne, J. T.,  
865 Croteau, P. L. and Robinson, A. L.: Secondary Organic Aerosol Formation from in-Use Motor Vehicle  
866 Emissions Using a Potential Aerosol Mass Reactor, *Environ. Sci. Technol.*, 48(19), 11235–11242,  
867 doi:10.1021/es502239v, 2014.

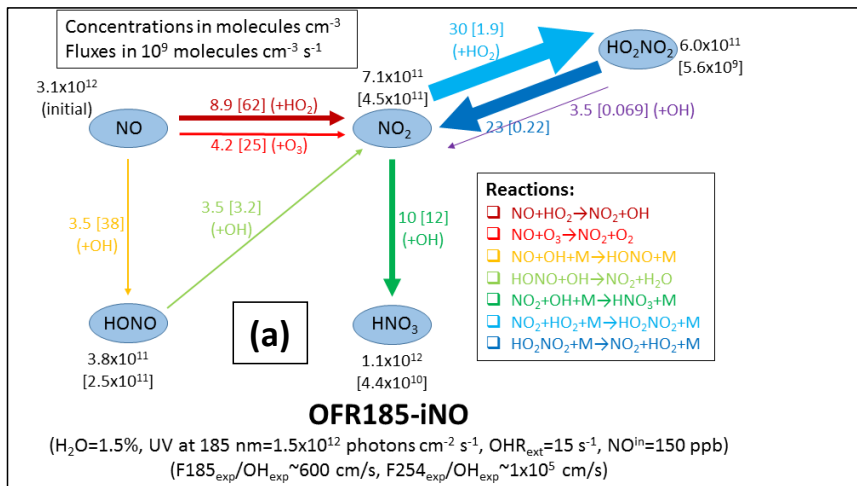
868 Volkamer, R., Jimenez, J. L., San Martini, F., Dzepina, K., Zhang, Q., Salcedo, D., Molina, L. T., Worsnop,  
869 D. R. and Molina, M. J.: Secondary organic aerosol formation from anthropogenic air pollution: Rapid  
870 and higher than expected, *Geophys. Res. Lett.*, 33(17), L17811, doi:10.1029/2006GL026899, 2006.

871 Wang, J., Doussin, J. F., Perrier, S., Perraudin, E., Katrib, Y., Pangu, E. and Picquet-Varrault, B.: Design of  
872 a new multi-phase experimental simulation chamber for atmospheric photochemistry, aerosol and cloud  
873 chemistry research, *Atmos. Meas. Tech.*, 4(11), 2465–2494, doi:10.5194/amt-4-2465-2011, 2011.

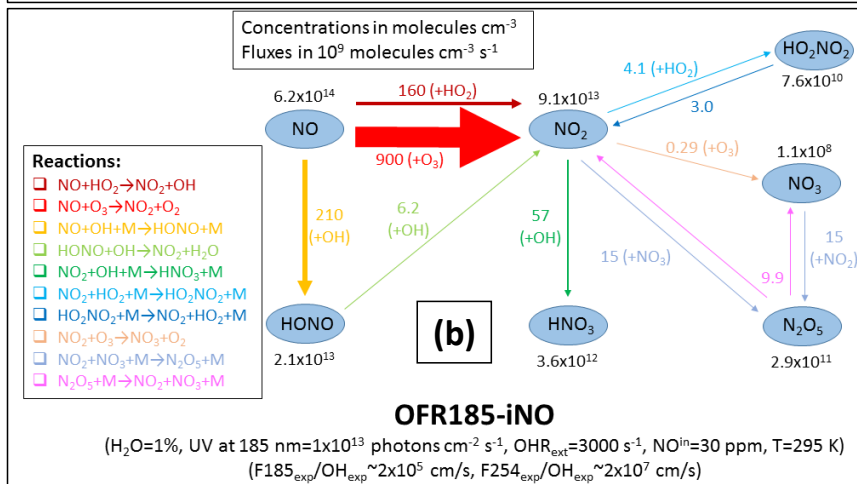
874 Zhang, X., Cappa, C. D., Jathar, S. H., McVay, R. C., Ensberg, J. J., Kleeman, M. J. and Seinfeld, J. H.:  
875 Influence of vapor wall loss in laboratory chambers on yields of secondary organic aerosol., *Proc. Natl.*  
876 *Acad. Sci. U. S. A.*, 111(16), 5802–7, doi:10.1073/pnas.1404727111, 2014.

877 Ziemann, P. J. and Atkinson, R.: Kinetics, products, and mechanisms of secondary organic aerosol  
878 formation, *Chem. Soc. Rev.*, 41(19), 6582, doi:10.1039/c2cs35122f, 2012.

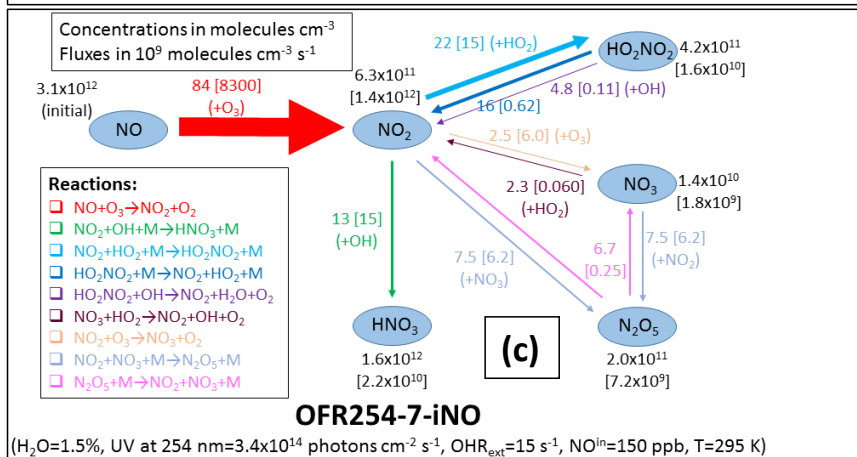
879



880

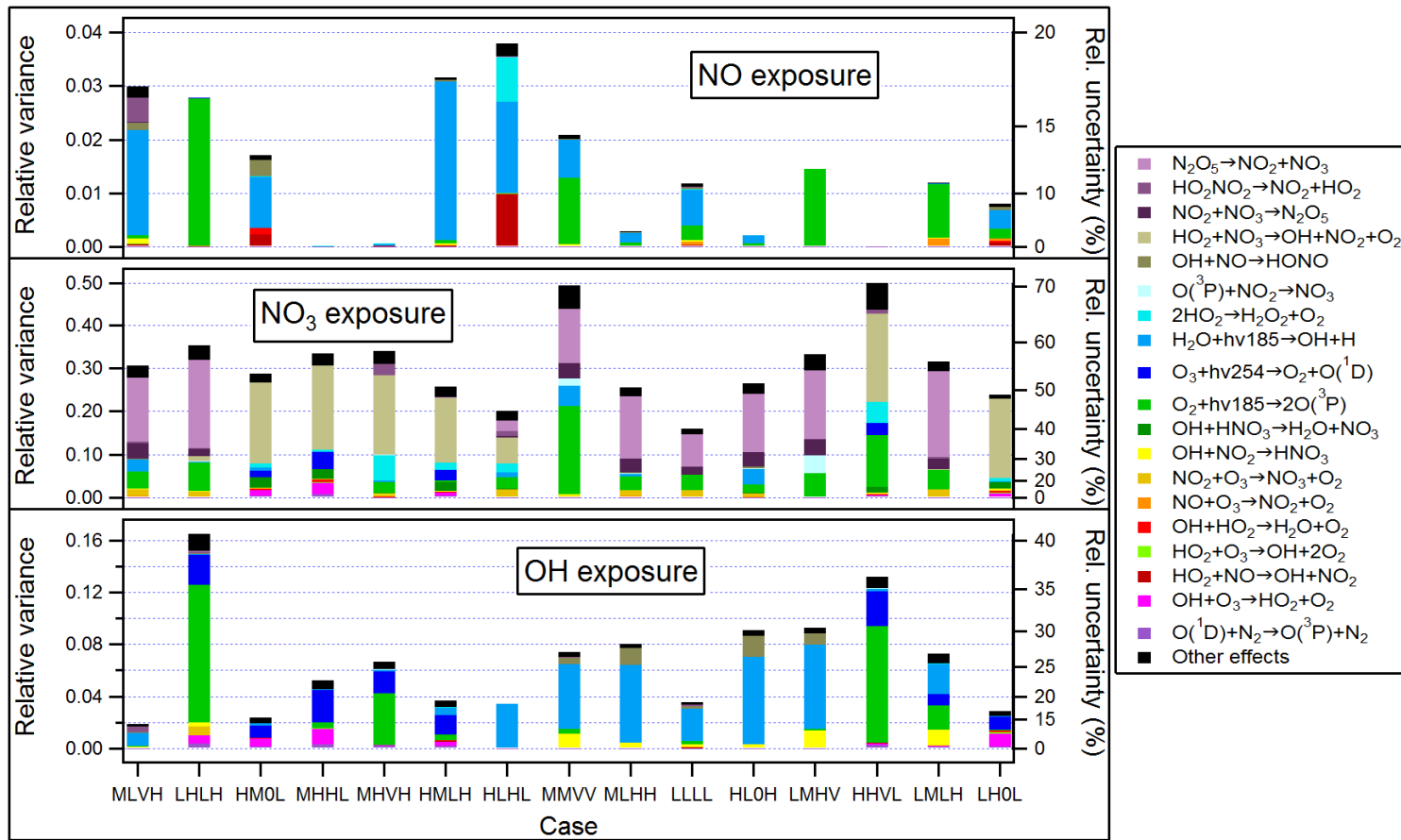


881



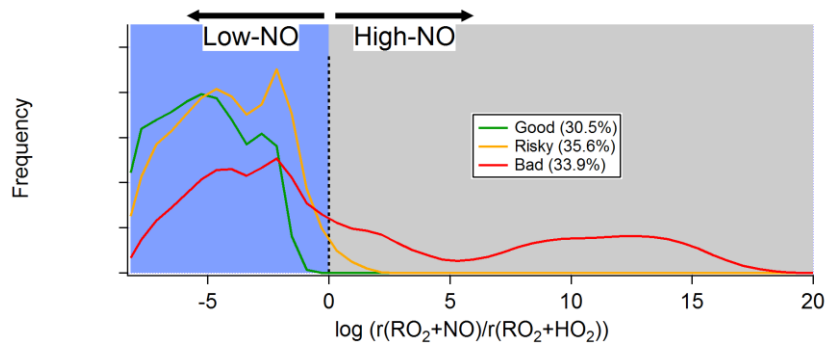
882

883 **Figure 1.** Schematics of main N-containing species and their major interconversion pathways under  
884 typical input conditions for (a) OFR185-iNO with  $\text{NO}^{\text{in}}=150$  ppb, (b) OFR254-7-iNO with  $\text{NO}^{\text{in}}=150$  ppb,  
885 and (c) OFR185-iNO with  $\text{NO}^{\text{in}}=30$  ppm. Species average concentrations (in molecules  $\text{cm}^{-3}$ ) are shown  
886 in black beside species names. Arrows denote directions of the conversions. Average reaction fluxes (in  
887 units of  $10^9$  molecules  $\text{cm}^{-3} \text{s}^{-1}$ ) are calculated according to the production rate, and shown on or beside  
888 the corresponding arrows and in the same color. Within each schematic, the thickness of the arrows is  
889 a measure of their corresponding species flux. Multiple arrows in the same color and pointing to the  
890 same species should be counted only once for reaction flux on a species. Note that all values in these  
891 schematics are average ones over the residence time, except for those in square brackets in panels a  
892 and b, which are average values within approximate NO effective lifetime ( $\tau_{\text{NO}}$ , or more accurately, an  
893 integer multiple of the model's output time step closest to NO effective lifetime). All concentrations and  
894 fluxes have two significant digits.



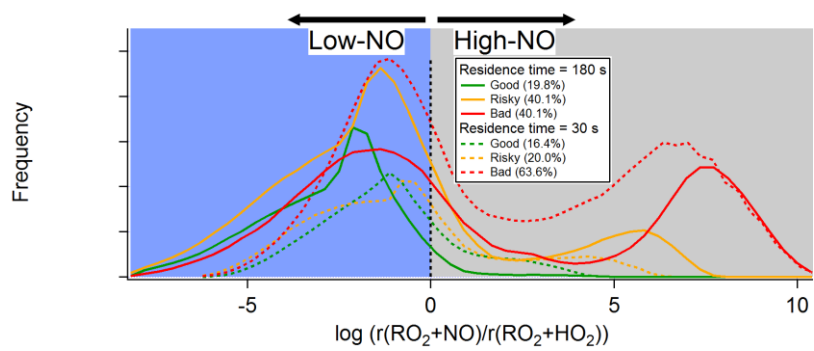
896 **Figure 2.** Relative variances (left axes)/uncertainties (right axes) of several outputs (i.e., NO, NO<sub>3</sub>, and OH exposures) of Monte Carlo uncertainty propagation, and relative  
897 contributions of key reactions to these relative variances in several typical cases (denoted in 4-character labels, see Table 2 for the typical case label code) in OFR185-iNO.  
898 Relative variances are shown in linear scales (left axis), while corresponding relative uncertainties, equal to relative variances' square roots, are indicated by the non-linear  
899 right axis. Only the reactions with a contribution of no less than 0.04 to at least one relative variance are shown.





900  
901

(a) OFR254-iNO

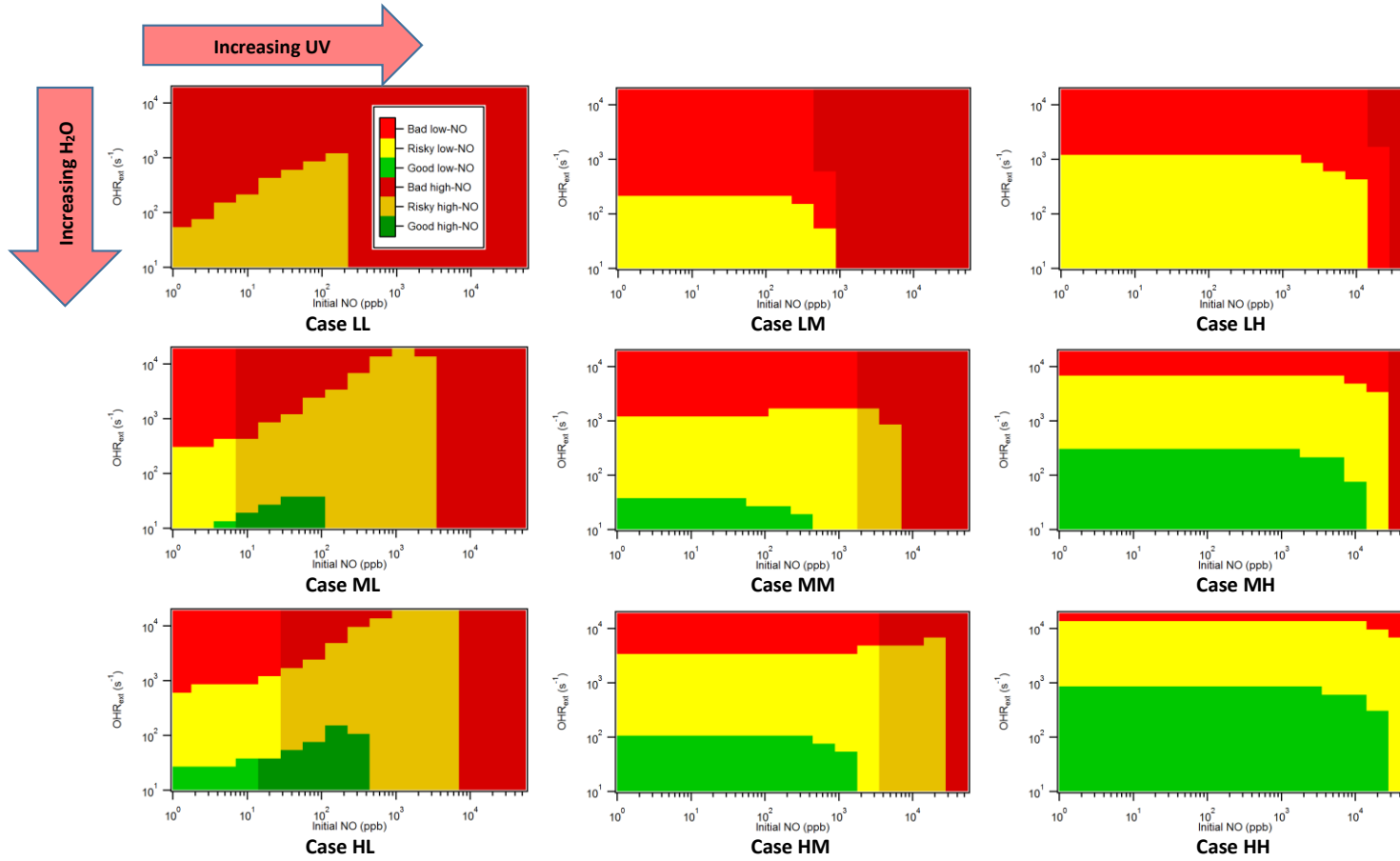


902  
903

(b) OFR185-iNO

904 **Figure 3.** Frequency occurrence distributions of good, risky, and bad conditions (see Table 3) over  
 905 logarithm of the ratio between  $\text{RO}_2$  reacted with NO and with  $\text{HO}_2$  (see Section S1 for more detail) for  
 906 (a) OFR254-iNO (only the case with a residence time of 180 s) and (b) OFR185-iNO (including two cases  
 907 with residence times of 180 and 30 s). Low and high-NO regions (see Table 3) are colored in light blue  
 908 and grey, respectively.

909  
910



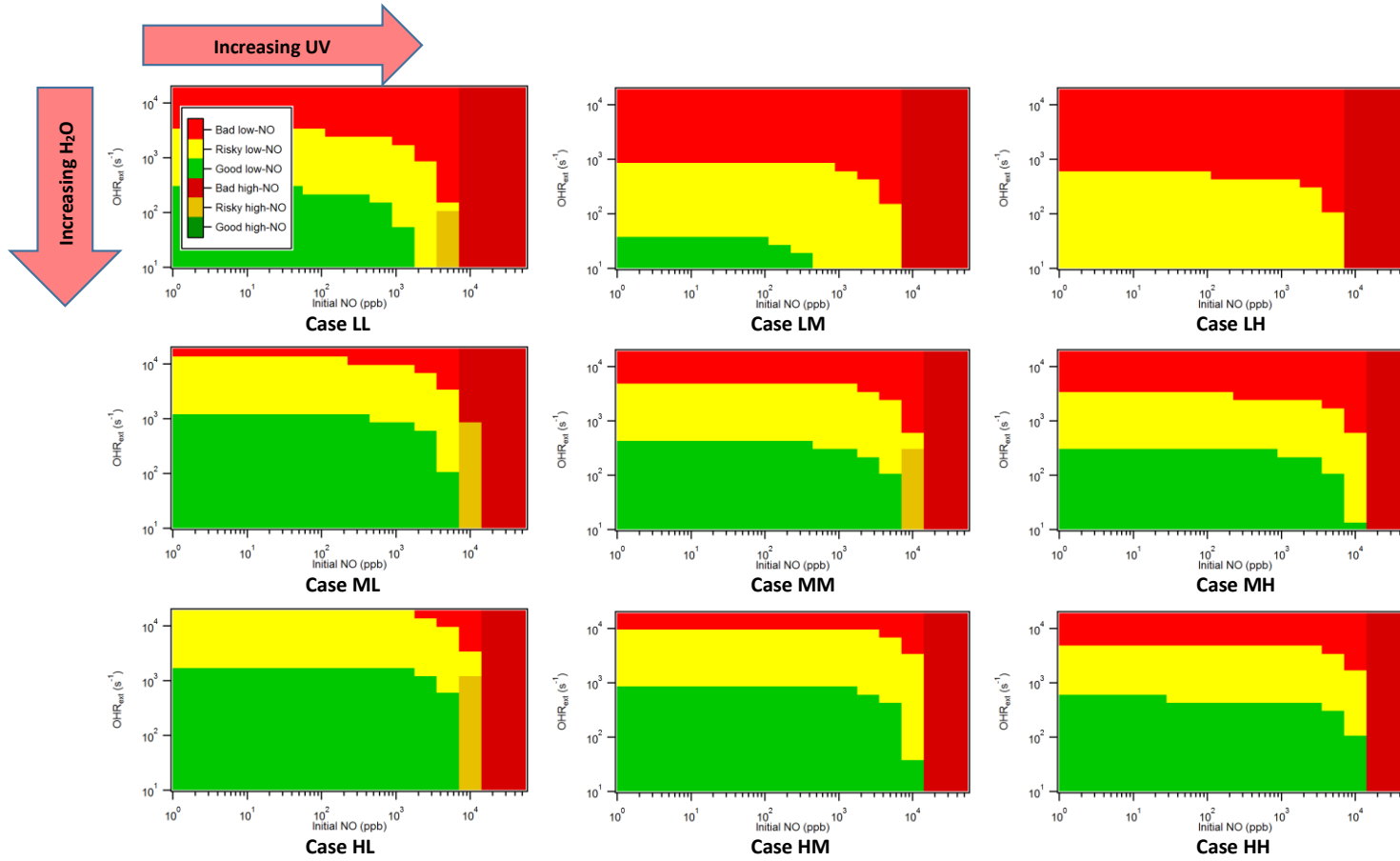
911  
912

913  
914

915  
916

917 **Figure 4.** Image plots of the condition types defined in Table 3 vs. external OH reactivity (excluding N-containing species) and initial NO for several typical cases in OFR185-  
918 iNO (see Table 2 for the case label code).  
919

920  
921

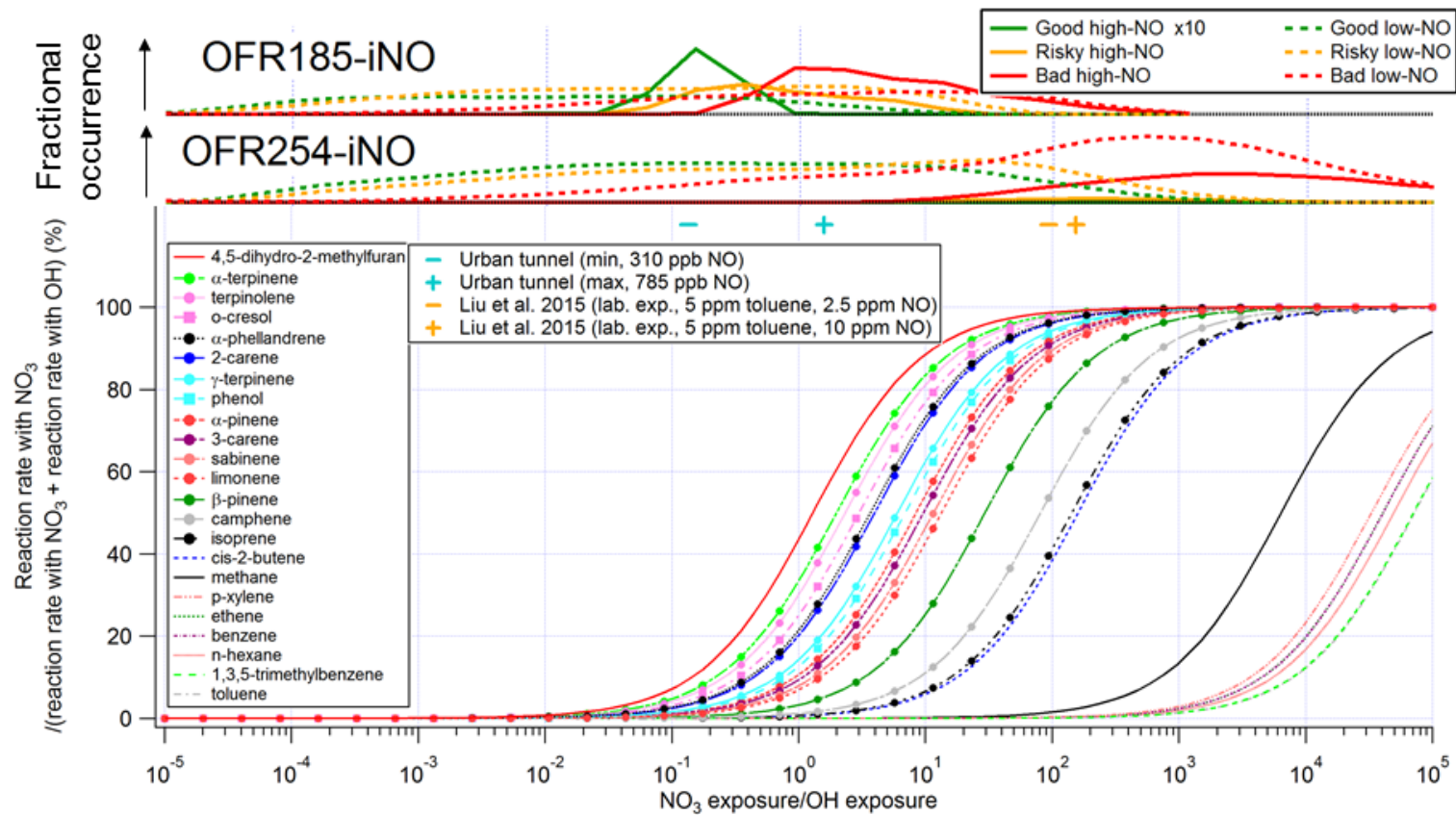


922  
923

924  
925

926  
927

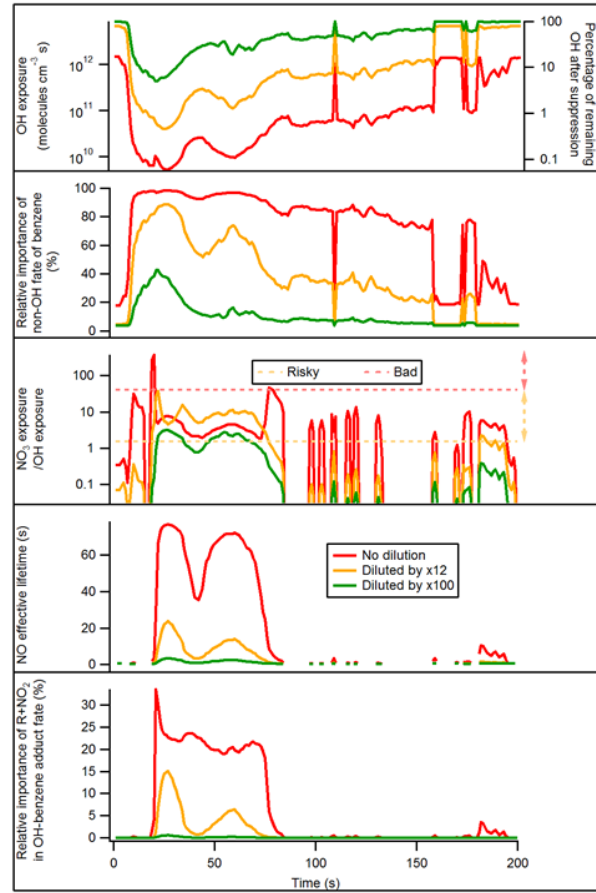
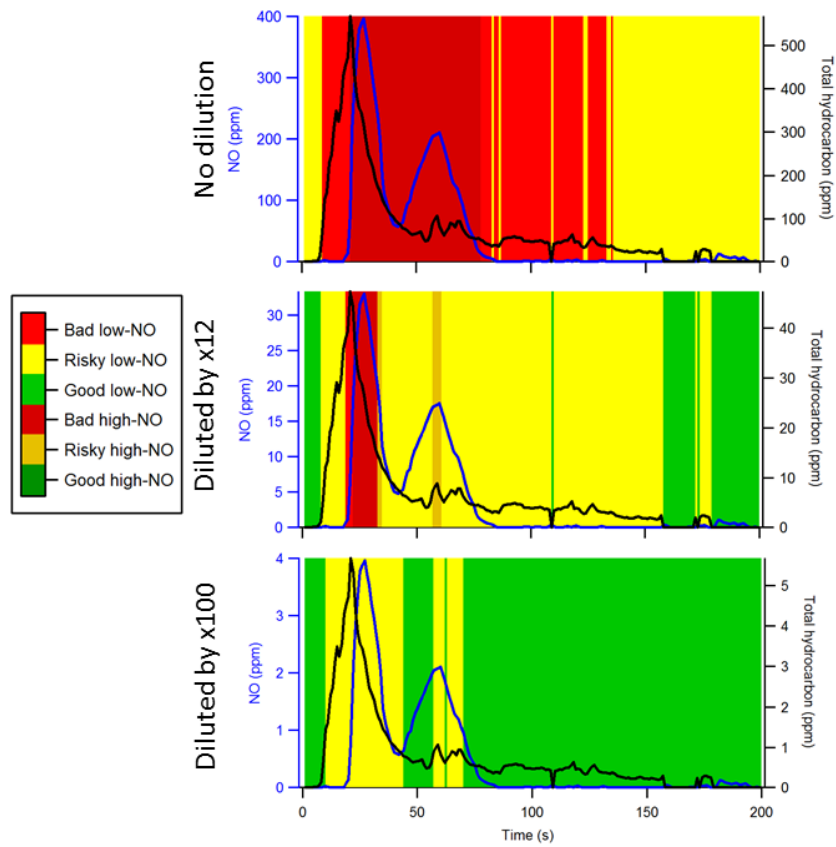
928 **Figure 5.** Same format as Fig. 4, but for OFR254-22-INO.



929  
930  
931

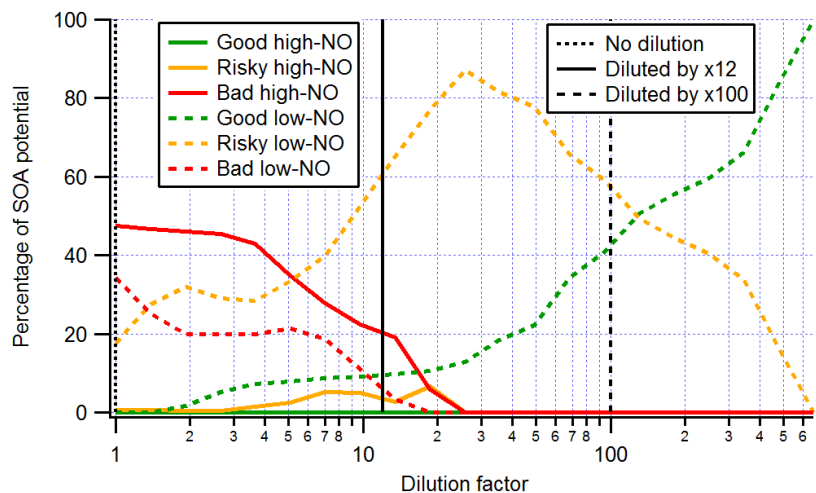
**Figure 6.** Fractional importance of the reaction rate of several species of interest with  $\text{NO}_3$  vs. that with OH, as a function of the ratio of exposure to  $\text{NO}_3$  and OH. The curves of biogenics and phenols are highlighted by solid dots and squares, respectively. The turquoise and orange markers show the ranges of modeled exposure ratios between  $\text{NO}_3$

932 and OH of a source study in an urban tunnel (Tkacik et al., 2014) and a laboratory study (Liu et al., 2015) using OFR, respectively. In the upper part of the figure, the modeled  
933 frequency distributions of ratios of NO<sub>3</sub> exposure to OH exposure under good/risky/bad high/low-NO conditions for OFR185-iNO and OFR254-iNO are also shown. See Table  
934 3 for the definitions of the three types of conditions. All curves, markers, and histograms in this figure share the same abscissa.  
935

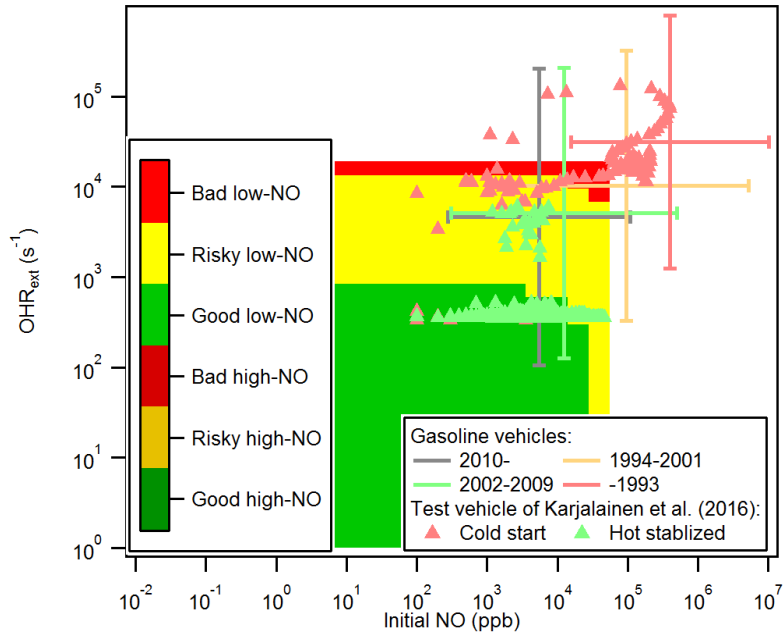




937 **Figure 7.** (left) NO and total hydrocarbon during the first 200 s of the test of Karjalainen et al. (2016) in the cases of no dilution, dilution by a factor of 12 (as actually done in  
938 that study), and dilution by a factor of 100. Different periods of time are colored according to corresponding emissions (i.e., input conditions for OFR), classified as  
939 good/risky/bad high/low-NO. (right) OH exposure/percentage of remaining OH after suppression, relative importance of non-OH fate of benzene, exposure ratio of NO<sub>3</sub> to  
940 OH, NO effective lifetime, and relative importance of reaction of OH-toluene adduct with NO<sub>2</sub> in the fate of this adduct in the OFR of Karjalainen et al. (2016) during the first  
941 200 s of their test in the cases of no dilution, dilution by a factor of 12, and dilution by a factor of 100. Horizontal orange and red dashed lines in the middle right panel denote  
942 “risky” and “bad” regions for exposure ratio of NO<sub>3</sub> to OH, respectively. Above the orange (red) dashed line, reaction with NO<sub>3</sub> contributes >20% to the fate of phenol (isoprene).



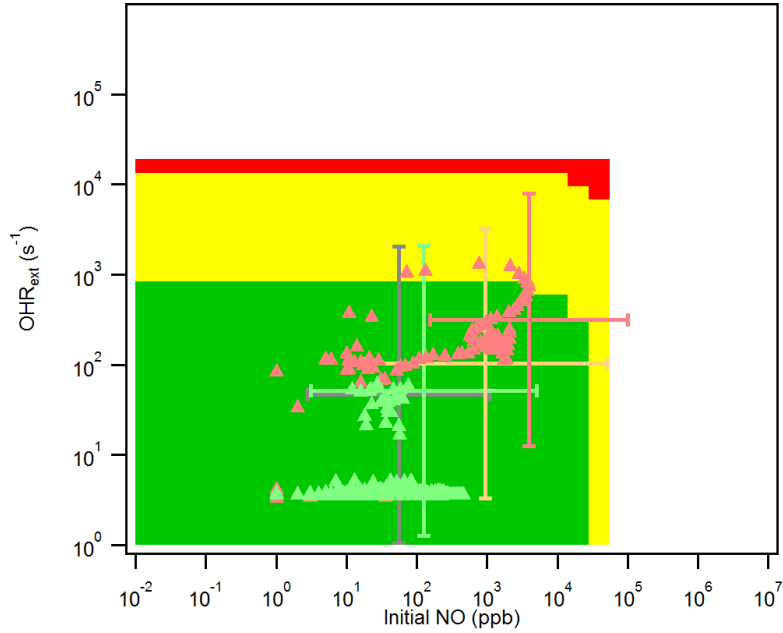
943  
 944 **Figure 8.** Secondary organic aerosol (SOA) potential (estimated from the total hydrocarbon  
 945 measurement) in the OFR of Karjalainen et al. (2016) formed during periods of time in the OFR  
 946 corresponding to good/risky/bad high/low-NO conditions, as a function of dilution factor. Vertical lines  
 947 denoting dilution factors of 1, 12 (as actually used in that study), and 100 are also shown.  
 948



949

950

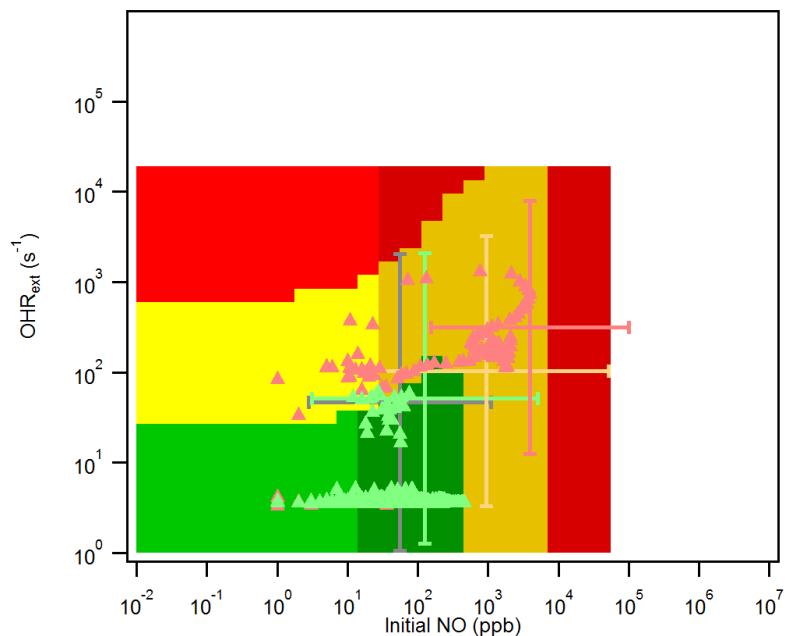
**(a) No dilution (background: Case HH)**



951

952

**(b) Dilution by a factor of 100 (background: Case HH)**



953

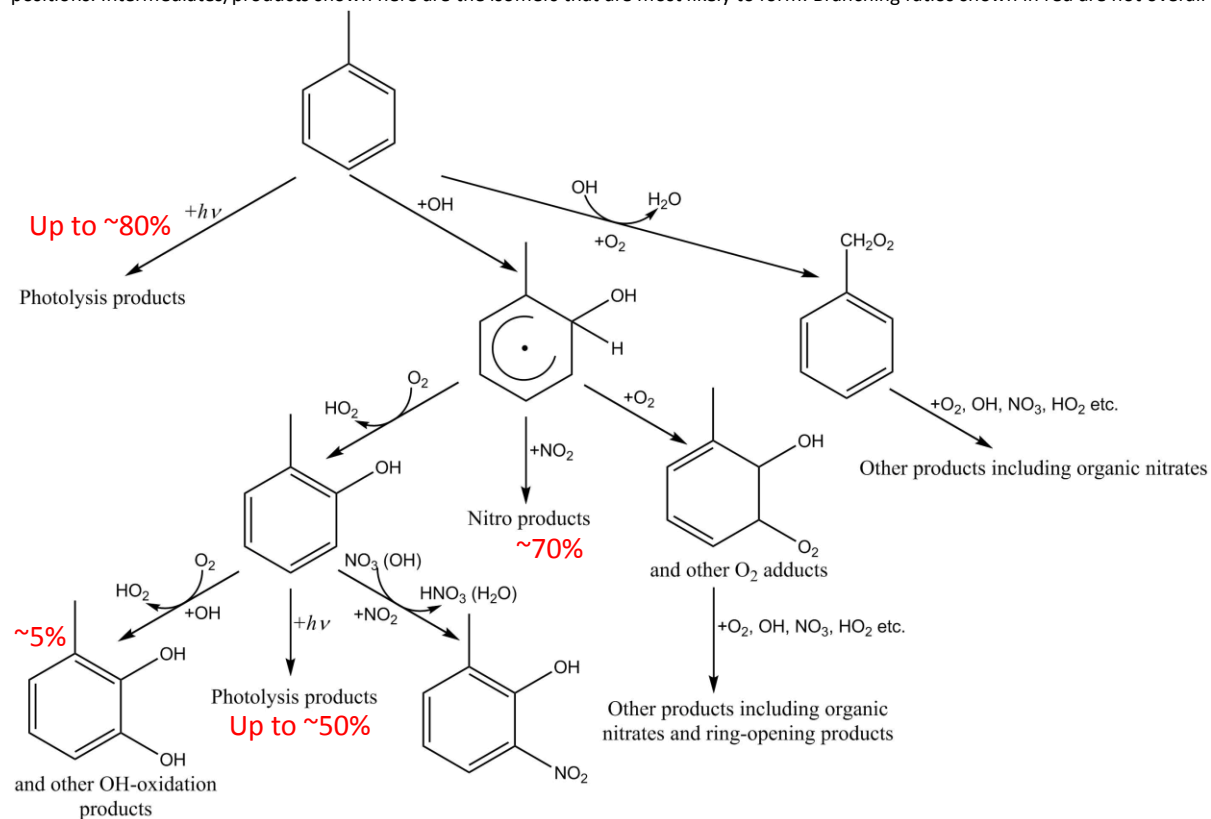
954

**(c) Dilution by a factor of 100 (background: Case HL)**

955 **Figure 9.** Location of individual 1 s datapoints vs. OFR185-iNO reaction conditions. Datapoints are shown  
 956 from the test vehicle of Karjalainen et al. (2016), as well as average exhaust from gasoline vehicle on-  
 957 road emissions measured by Bishop and Stedman (2013). On-road emissions are classified by vehicle  
 958 year and the distribution of each category is shown as a cross representing 1 standard deviation (with  
 959 log-normal distribution assumed). The X and Y axes are NO and external OH reactivity (excluding N-  
 960 containing species) due to vehicle emissions in OFR in the cases of (a) no dilution and (b,c) dilution by a  
 961 factor of 100. The Karjalainen et al. (2016) points are classified as cold start (during first 200 s) and hot  
 962 stabilized (during 200–1000 s). In addition, the same image plots as the panels of Cases HH (high H<sub>2</sub>O  
 963 and high UV, see Table 2 for the case label code) and HL in Fig. 4 (OFR185-iNO) are shown as background  
 964 for comparison.

965

966 **Scheme 1.** Possible major reactions in an OFR254-13-iNO with 5 ppm toluene and 10 ppm initial NO. Branching ratios in red are estimated by the model and/or according to  
 967 Calvert et al. (2002), Atkinson and Arey (2003), Ziemann and Atkinson (2012), and Peng et al. (2016). Note that addition/substitution on the aromatic ring may occur at other  
 968 positions. Intermediates/products shown here are the isomers that are most likely to form. Branching ratios shown in red are not overall but from immediate reactant.



969

970

**Table 1.** Experimental conditions of several OFR studies with high NO injection.

Study	Source type	Temperature (K)	Relative humidity (%)	Dilution factor	External OH reactivity of undiluted source ( $s^{-1}$ )	Source NO <sub>x</sub> concentration (ppm)
Link et al. (2016)	Diesel vehicle emission		50	45–110	$\sim 5000^{*1}$	$436^{*1}$
Martinsson et al. (2015)	Biomass burning emission			1700	$156400^{*1}$	154
Karjalainen et al. (2016)	Gasoline vehicle emission	295	60	12	$\sim 73000^{*2,a}$	$\sim 400^{*1,b}$
Liu et al. (2015)	Purified gas	293	13	1	$\sim 1400^{*1,a}$	$10^{*1,b}$
Tkacik et al. (2014)	Tunnel air	293	42	1	$\sim 60^{*1,a}$	$\sim 0.8^{*1}$
Ortega et al. (2013)	Biomass burning emission	290	30	$\sim 500$	$\sim 15-500$	$\sim 0.2$

971  
972  
973  
974  
975<sup>\*1</sup> maximum value in the study<sup>\*2</sup> value at the moment of maximum NO emission<sup>\*a</sup> NO<sub>y</sub> species excluded<sup>\*b</sup> NO only

976 **Table 2.** Code of the labels of typical cases. A case label can be composed of four characters denoting the water mixing ratio, the photon flux, the external OH reactivity  
 977 excluding N-containing species, and the initial NO mixing ratio, respectively. A case label can also be composed of two characters denoting the water mixing ratio and the  
 978 photon flux.

	Water mixing ratio	Photon flux	External OH reactivity (no ON)	Initial NO mixing ratio
Options	L=low (0.07%)	L=low ( $10^{11}$ photons $\text{cm}^{-2} \text{s}^{-1}$ at 185 nm; $4.2 \times 10^{13}$ photons $\text{cm}^{-2} \text{s}^{-1}$ at 254 nm)	0	0
	M=medium (1%)	M=medium ( $10^{13}$ photons $\text{cm}^{-2} \text{s}^{-1}$ at 185 nm; $1.4 \times 10^{15}$ photons $\text{cm}^{-2} \text{s}^{-1}$ at 254 nm)	L=low ( $10 \text{ s}^{-1}$ )	L=low (10 ppb)
	H=high (2.3%)	H=high ( $10^{14}$ photons $\text{cm}^{-2} \text{s}^{-1}$ at 185 nm; $8.5 \times 10^{15}$ photons $\text{cm}^{-2} \text{s}^{-1}$ at 254 nm)	H=high ( $100 \text{ s}^{-1}$ )	H=high (316 ppb)
			V=very high ( $1000 \text{ s}^{-1}$ )	V=very high (10 ppm)
Example	LH0V:	low water mixing ratio, high photon flux, no external OH reactivity (excluding ON), very high initial NO mixing ratio		
	ML:	medium water mixing ratio, low photon flux		

979  
980

981 **Table 3.** Definition of condition types in this study (good/risky/bad high/low-NO).

Condition	Good	Risky	Bad
Criterion	$F_{185_{\text{exp}}}/OH_{\text{exp}} < 3 \times 10^3 \text{ cm s}^{-1}$ and $F_{254_{\text{exp}}}/OH_{\text{exp}} < 4 \times 10^5 \text{ cm s}^{-1}$	$F_{185_{\text{exp}}}/OH_{\text{exp}} < 1 \times 10^5 \text{ cm s}^{-1}$ and $F_{254_{\text{exp}}}/OH_{\text{exp}} < 1 \times 10^7 \text{ cm s}^{-1}$ (excluding good conditions)	$F_{185_{\text{exp}}}/OH_{\text{exp}} \geq 1 \times 10^5 \text{ cm s}^{-1}$ or $F_{254_{\text{exp}}}/OH_{\text{exp}} \geq 1 \times 10^7 \text{ cm s}^{-1}$
Condition	High-NO	Low-NO	
Criterion*	$\frac{r(\text{RO}_2 + \text{NO})}{r(\text{RO}_2 + \text{HO}_2)} > 1$	$\frac{r(\text{RO}_2 + \text{NO})}{r(\text{RO}_2 + \text{HO}_2)} \leq 1$	

\* See Section S1 for detail.

982  
983



984 **Table 4.** Statistics of the ratio between OH exposures calculated in the model with the Lambe et al. (2011) residence time distribution ( $OH_{exp,RTD}$ ) and in the plug-flow model  
985 ( $OH_{exp,PF}$ ). The geometric mean, uncertainty factor (geometric standard deviation), and percentage of outlier cases ( $>3$  or  $<1/3$ ) are shown for OFR185-iNO, OFR254-70-iNO,  
986 and OFR254-7-iNO.

	Geometric mean	Uncertainty factor	Outlier cases (%)
OFR185-iNO	1.91	1.64	11
OFR254-7-iNO	1.59	1.51	7
OFR254-70-iNO	1.48	1.29	3

987